TECHNISCHE UNIVERSITÄT WIEN

DIPLOMARBEIT

Stability of Functionalised Supported Lipid Bilayers at Ambient and Physiological Temperatures

zur Erlangung des akademischen Grades
Diplom-Ingenieurin

im Rahmen des Studiums
Biomedical Engineering

ausgeführt am Institut für Angewandte Physik der Fakultät Physik in der Forschungsgruppe für Biophysik
der Technischen Universität Wien

unter der Anleitung von

Univ.Prof. Dipl.-Ing. Dr.techn. Gerhard Schütz,

Dipl.-Ing. Dr.techn. Mario Brameshuber

und

Caroline Kopittke, MSc

durch

Anna Gaugutz, BSc
Matrikelnummer: 51830960

Wien, 15.05.2022

Unterschrift Betreuer

Unterschrift Verfasserin

Zusammenfassung

Lipid-Doppelschichten auf festem Substrat (SLBs) werden mit pMHC-Molekülen funktionalisiert, welche über His-Tags an Ni-chelatierende Lipide gebunden sind, um die Aktivierung von T Zellen zu untersuchen. Stabile Proteinbindung und gute Membranqualität sind dafür über lange Zeit während Experimenten wichtig. In dieser Arbeit wurde die Bindungsstabilität von His-markierten Proteinen in Abhängigkeit der Anzahl an Tags bei zwei Temperaturen analysiert.

SLBs (98% POPC/2% DGS-NTA(Ni)) wurden mit IE^K (zwei His-Tags) und Streptavidin (ein/zwei/drei His-Tags) funktionalisiert. Die Stabilität der Bindung wurde bei 21°C und 37°C mittels TIRF-Mikroskopie analysiert und Proteinoberflächendichten wurden über die Zeit berechnet. Es wurde ein Desorptions-Modell entwickelt und die Off-Raten wurden bestimmt.

Bei 21°C blieben die Proteine auf der Lipidmembran mobil, obwohl eine Abnahme in der Dichte zu sehen war. Mit zunehmender Anzahl von His-Tags blieb die Bindung stabiler und führte zu geringeren Off-Raten. Bei 37°C dissoziierten die Proteine schneller und innerhalb von $2 - 2,5$ Stunden waren nur noch unbewegliche Aggregate vorhanden. Die Off-Raten nahmen zu und lagen für jedes Protein in der gleichen Größenordnung. Dennoch konnte eine Verbesserung der Bindungsstabilität erreicht werden, indem der pH-Wert des Puffers erhöht wurde. Wesentlich langsamere Desorption wurde für IE^K bei 37°C beobachtet.

Zusammenfassend lässt sich feststellen, dass die Proteinoberflächendichte sowohl bei 21°C als auch bei 37°C abnahm. Da der pH-Wert des Puffers die koordinative Bindung zwischen His-Tags und Ni-Ionen beeinflussen kann, müssen experimentelle Bedingungen sorgfältig gewählt werden.

Abstract

Supported lipid bilayers (SLBs) are functionalised with pMHC molecules, that are bound through His-tags to Ni-chelated lipids to study the activation behaviour of T cells. Consequently, stable protein binding and bilayer quality are important over long periods of time during experiments. In this thesis, the binding stability of His-tagged proteins has been determined in dependence on the number of tags at two temperature conditions.

SLBs (98% POPC/2% DGS-NTA(Ni)) were functionalised with IE^K (two His-tags) and Streptavidin (one/two/three His-tags). The stability of binding was observed at 21°C and 37°C with TIRF microscopy and protein surface densities were calculated over time. A desorption model was developed and off-rates were determined.

At 21°C proteins stayed mobile on bilayers, although a decrease in density could be observed. With increasing number of His-tags binding was more stable and resulted in smaller off-rates. At 37°C proteins rapidly dissociated and only immobile aggregations were present within $2 - 2.5$ hours. Off-rates increased and were in the same order of magnitude for each protein. Nevertheless, an improvement in binding stability could be achieved by increasing the pH of the buffer. Much slower desorption of IE^K was observed at 37°C.

In conclusion, protein surface densities decreased both at 21°C and 37°C. Since the pH of the buffer may interfere with the coordination bond between His-tags and Ni-ions, experimental conditions must be chosen carefully.

Acknowledgements

This thesis represents a big step in my academic journey. I have learned so much during my work on this project and it would not have been possible without several people.

First, I would like to thank Gerhard Schütz for giving me the opportunity to do my thesis within the Biophysics Group at the Technical University of Vienna.
My deepest gratitude goes to Caroline Kopittke and Mario Brameshuber. Thank you for your guidance through my research for a lot of helpful discussions, constructive feedback and kind supervision.

Furthermore, I would like to thank the whole Biophysics Group for welcoming me into your team and for creating such an enjoyable working atmosphere. In particular I would like to mention Marina Bishara und Lukas Schrangl for helping me with part of the analysis and Simon Jaritz, who helped with two schematics for this thesis. It has been a pleasure to work within the group and I am looking forward to continue beeing part of your team in the future.

Finally, I want to thank my parents, Martina and Peter Gaugutz, for supporting me through all my life and never stopping to believe in me. Special thanks go also to my sister Julia and my friends, who were always there for me with an open ear and encouraging words.

Eidesstaatliche Erklärung

Ich erkläre an Eides statt, dass die vorliegende Arbeit nach den anerkannten Grundsätzen für wissenschaftliche Abhandlungen von mir selbstständig erstellt wurde. Alle verwendeten Hilfsmittel, insbesondere die zugrunde gelegte Literatur, sind in dieser Arbeit genannt und aufgelistet. Die aus den Quellen wörtlich entnommenen Stellen, sind als solche kenntlich gemacht. Das Thema dieser Arbeit wurde von mir bisher weder im In- noch Ausland einer Beurteilerin/einem Beurteiler zur Begutachtung in irgendeiner Form als Prüfungsarbeit vorgelegt. Diese Arbeit stimmt mit der von den Begutachterinnen/Begutachtern beurteilten Arbeit überein.

Wien, 15.05.2022

Signature

Contents

1. Introduction

All living organisms are connected with their environment. They need to interpret and react to exogenous stimuli and other sensory impressions by adjusting their behaviour. This ability is essential for survival and requires a network of molecules and cells interacting and communicating with each other. Even the most primitive cell monitors its environment and responds to countless of signals. These signals are transferred by signalling molecules that are either released from the signalling cell or remain bound to its membrane surface. The latter, contact-depending form is particularly important in immune responses. [1, 2]

Microbes, like bacteria, germs or viruses, threaten host functions by replicating and spreading inside the body. After entering through the epithelia, they are captured by antigen-presenting cells (APCs). APCs process them and display the peptide fragments bound to major histocompatibility complex (MHC) molecules on their surface. The cells migrate to lymphoid organs, where the peptide-MHC (pMHC) complex is recognised by T lymphocytes. [2–4] A common response to infection by such microbes is fever. Increased body temperatures trigger different pathways of the immune response, for instance lymphocyte response to stimulatory signals is enhanced. Consequently, febrile temperatures are associated with increased effectiveness of the immune system and improved organism survival. [5] However, T cell activation at different temperature ranges, such as physiological or febrile temperatures, is still a topic of ongoing research [6–9].

Since it is nearly impossible to study the behaviour of T lymphocytes in their natural environment inside the body, model systems are necessary that enable the investigation of T cell activation. A widely used experimental model to study this mechanism is a supported lipid bilayer (SLB). SLBs mimic cell membranes by forming a single phospholipid bilayer on a solid surface. In 1985, Tamm et al. [10] developed the first membrane on solid support. Since than, these model systems have been employed in a wide range of biological and biotechnological applications, due to their many advantages. SLBs offer a controlled, stable substrate, that maintains the lateral fluidity of biomembranes. Furthermore, lipid composition can be individually adjusted and proteins can be integrated into the bilayer. [11–13]

Integrating proteins while still preserving the fluid behaviour of biological membranes is a challenging task. Nevertheless, it can be achieved by using metal-chelated lipids that bind proteins via affinity tags. Such affinity tags are typically

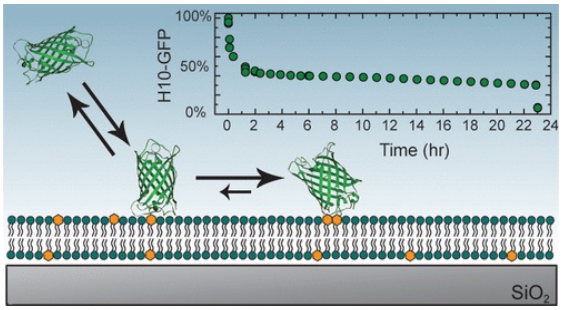

Figure 1.1.: Proposed desorption mechanism by Nye et al. [18] Polyvalently bound His-tagged GFP remains bound on the bilayer for several hours. The polyvalent species slowly transitions into monovalently bound proteins, which rapidly dissociate from the bilayer. The graph shows the remaining percentage of bound GFP over the course of 23 hours.

used in protein purification systems and consist of amino acids. One of the most popular residues is histidine (His). The binding to metal ions is accomplished by the imidazole side chains of individual His residues. They form stable coordination bonds with Ni^{2+} chelated to nitrilotriacetic acid (NTA). [14–17]

The binding stability of His-tagged proteins on a SLB has been investigated by Nye et al. [18]. The density of green fluorescent protein (GFP) tagged with 10 His residues was monitored over 23 hours (Figure 1.1). After an initial drop during the first two hours to around 40% of proteins remaining on the bilayer, slow desorption can be seen. They proposed a two step unbinding model, in which polyvalently bound proteins slowly transition into monovalently bound species, that rapidly dissociate. However, the exact mechanism remains still unknown.

Influences on the binding stability have been studied with surface plasmon resonance. Measurements including uncoupled tags with a different number of His residues (ranging from dihistidine to decahistidine) showed that increasing the number of His leads to slower desorption rates and binding is more stable. However, hexahistidine has the highest binding affinity towards Ni-NTA and thus provides the optimal length. [19] The stability can also be increased by adding more His-tags to proteins and taking advantage of the avidity effect. [20] Another possible way to achieve improved binding stability is by using multidentate chelator headgroups, such as trivalent nitrilotriacetic acid (trisNTA). Compared to monovalent NTA, trisNTA decreases dissociation rates of oligohistidines [21] and increases the fraction of proteins that remains bound to liposomes containing trisNTA-lipids over several hours [22]. However, the effect on the binding of His-tagged proteins to SLBs containing trisNTA-lipids has not been investigated so far.

To sum up, the exact binding mechanism is still not fully understood and is affected by many aspects, such as the number of residues as well as the number of

tags. The influence of these two factors has only been studied over short periods, but not for prolonged time over several hours on membrane surfaces. Furthermore, the effect of physiological temperature on SLBs and the binding between His-tagged proteins and Ni-chelated lipids has not been reported in literature so far. To prevent potential influences from altering experimental outcomes, stable protein binding and bilayer quality are important. Thus, it is of great interest to gain more insight about how the stability of functionalised SLBs is affected by proteins with a different number of His-tags as well as how the behaviour changes at physiological temperature.

Aim

The aim of this thesis is to determined the stability of SLBs functionalised with various proteins at two temperature conditions, namely room temperature (21°C) and in physiological condition (37°C). Emphasis will be given on the desorption behaviour depending on the number of His-tags, since proteins with either one, two or three tags are used in the experiments. The stability is assessed over several hours by means of protein mobility and surface density as well as with a tracer lipid to characterise the behaviour of the bilayer itself. Since this topic has scarcely been reported in literature, further insight may help to improve experimental methods involving His-tagged proteins.

2. Theoretical Background

2.1. Supported Lipid Bilayers

Biological membranes play a crucial role in many cellular processes, including signalling mechanisms, the transport of molecules between the intra- and extracellular space and the participation in various other processes both inside and outside of the cell. [11] Consequently, model systems are necessary to study such interactions. One of the most widely used membrane mimics are supported lipid bilayers (SLBs), which form a single phospholipid bilayer on a solid support. They offer the advantages of a controlled, stable substrate, which can be studied with various surface-sensitive measurement techniques. Furthermore, SLBs provide an excellent environment to integrate membrane proteins and allow free translational and rotational diffusion of lipids, thus maintaining the fluidity of biomembranes. [11–13] The latter characteristic is caused by a $10 - 20$ Å layer of water between the lower leaflet of the bilayer and the solid support (Figure 2.1) [23, 24]. An important characteristic for the fluidity is the phase of the lipids. Generally, lipid bilayers can realise reversible phase transitions between ordered gel-states (L_β) and disordered liquid-crystalline phases (L_α). They result in changes of lattice order (solid or liquid) and lipid chains (ordered or disordered). Melting from the L_β to the L_α phase is accompanied with an increase in bilayer area and a decrease in bilayer thickness. The transition depends on different parameters, such as temperature, pressure, pH and ionic strength. Temperature induced (thermotropic) changes have been widely studied. The temperature at which the conversion occurs is known as the phase transition temperature T_M and depends on the type of lipid. [25–27] Litman et al. [28] determined T_M for 1-palmitoyl-2-oleoyl-glycero-3-phosphocholine (POPC) around -3°C, which consequently does not influence experiments in ambient or physiological temperature conditions.

Different methods have been established to create SLBs. In 1985 the first membrane on solid support was developed by Tamm et al. [10]. They deposited a lipid bilayer on a hydrophilic substrate by attaching two monolayers from an air-water interface in two sequential steps. The first monolayer was taken up by pushing the hydrophilic surface through the air-water interface at a 90° angle. Afterwards, the coated substrate was apposed horizontally to the air-water interface and pushed through again.

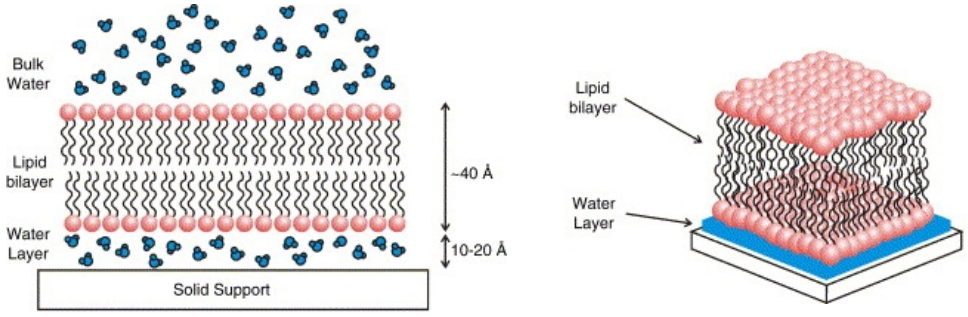

Figure 2.1.: Diagram of a SLB on solid support. The substrate and the membrane are separated by a $10-20$ Å layer of water responsible for the fluidity of the bilayer. [24]

Since then, SLBs have become popular in a variety of biological applications, for instance to study membrane properties [29], protein functions like enzyme activities [30] or protein-receptor interactions, such as antigen recognition by T cells [31], but they are also used in biotechnological applications like biosensors [32].

Popular fabrication approaches include Langmuir techniques and vesicle fusion. The latter offers the most convenient way, since it generates high-quality bilayers in a simple, one-step procedure. The underlying process of bilayer formation can be explained by several steps (Figure 2.2) [11, 33–35]:

1. **Adsorption:** isolated vesicles adsorb on the solid support, due to a combination of van der Waals attractions, electrostatic interactions and hydration forces.

2. **Deformation:** surface-induced flattening leads to the deformation of vesicles, which increases stress.

3. **Fusion:** some of the vesicles fuse and form larger ones.

4. **Rupture:** when the stress becomes sufficient, vesicles rupture and the SLB is formed by lateral spreading of the membrane.

Several factors influence this process, such as the vesicles themselves (their size, charge, composition and physical state), the aqueous solution (its composition, ionic strength and pH) and the solid support (its roughness, surface charge and composition). Successful bilayer formation involves sonication of the lipid mixture as well as plasma cleaning of the support to make the surface hydrophilic. [24]

Binding and stability of vesicles have been widely studied. Lipowsky and Seifert [36] developed a theoretical model, where adsorption, deformation and rupture are determined by a balance between adhesion energy and curvature energy.

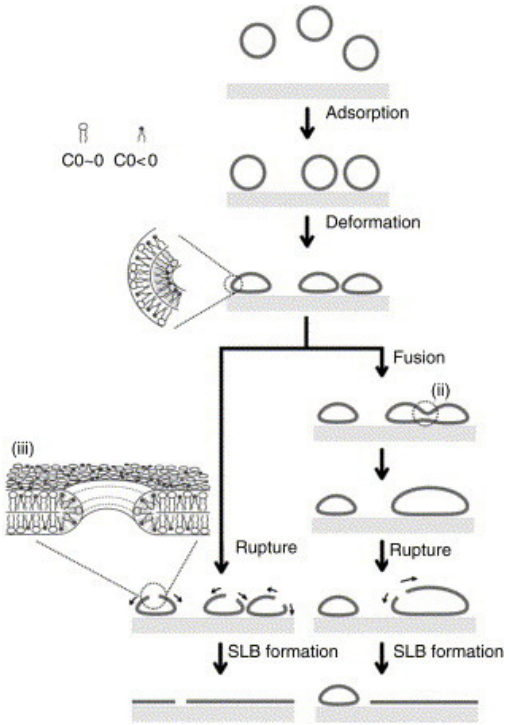

Figure 2.2.: Bilayer formation by vesicle fusion. Vesicles adsorb on the support and flattening at the surface leads to the deformation of vesicles. Prior to vesicles rupture an intermediate step can occur, where some of the vesicles fuse. Finally, the bilayer spreads on the solid support. [35]

However, also intervesicular cooperative effects have to be taken into account. When the surface density of vesicles is too low, rupture might not occur. Richter et al. [11] observed stable adsorption of intact vesicles for several days below a critical density in atomic force microscopy measurements. In contrast, when a critical surface coverage was reached, the vesicles were forced into contact. Contact leads to increased stress, which induces fusion and rupture. The exposed edges of the ruptured membranes are energetically unfavourable and promote the interaction with neighbouring vesicles, thereby leading to a chain of rupture events and the formation of the bilayer on the substrate. [11]

2.2. Interaction of His-tagged proteins with Nickel chelated lipids

Integrating proteins into SLBs while still maintaining two-dimensional fluidity is a challenging task. A method to accomplish this, is by using metal-chelated lipids,

which bind soluble proteins to the bilayer via affinity tags. [18] The binding bases on the formation of a coordination bond between metal ions, like Cu^{2+}, Zn^{2+} or Ni^{2+} [37], and specific side chains of amino acids, such as cysteine (Cys), arginine (Arg) or histidine (His) on the affinity tag. In this interaction, the metal ions participate as electron-pair acceptors (Lewis acid) and the amino acid ligands as electron-pair donors (Lewis base). [14]

2.2.1. His-tags in protein purification systems

Such affinity tags are typically used for immobilisation in protein production and purification systems. The first ones who used His-tags for protein purification were Hochuli et al. [15] in 1987. They developed a quadridentate metal chelating adsorbent based on a derivative of nitrilotriacetic acid (NTA). The NTA resin occupies four valencies in the octahedral coordination sphere of the metal ion, thereby leaving two sites free for protein interactions. Furthermore, they observed stronger binding when the tag consisted of two neighbouring His residues. [15] In 1988 Hochuli et al. [16] successfully purified an enzyme with a poly His-tag. They discovered that increasing the number of His residues leads to a lower amount of eluted protein under physiological conditions in phosphate buffer, which consequently indicates that the binding is stronger.

Since this pioneering work [16, 17], His-tags have become one of the most widely used peptide tags. They are usually comprised of six consecutive His residues (Figure 2.3), which offers high selectivity since oligohistidine segments are rather rare in nature. [19] Compared to other amino acids, His-tags form more stable chelates due to their imidazole side-chains. [14] Additionally, they offer great flexibility in the location of the tag, as they can be attached to the C-terminus, the N-terminus or both, depending on the type of protein. [17, 38] Disparity exists whether the His-tag alters the structure of the protein; some groups claim no or minimal influence [17, 39], whereas others observed changes in the structure [40]. Nevertheless, in neither case was the function impaired. Another advantage for protein purification systems is the reversibility of the interaction. There are different protocols which can be employed for the elution of proteins: ligand exchange, protonation or chelate annihilation. Ligand exchange can be achieved with a competing electron donor like imidazole. Reducing the pH leads to the protonation of the electron donor group which reverses the coordination bond. Chelate annihilation can be done by adding a strong chelating agent like ethylenediaminetetraacetic acid (EDTA), which strips the Ni^{2+} ions from the NTA adsorbent. [14, 17, 38]

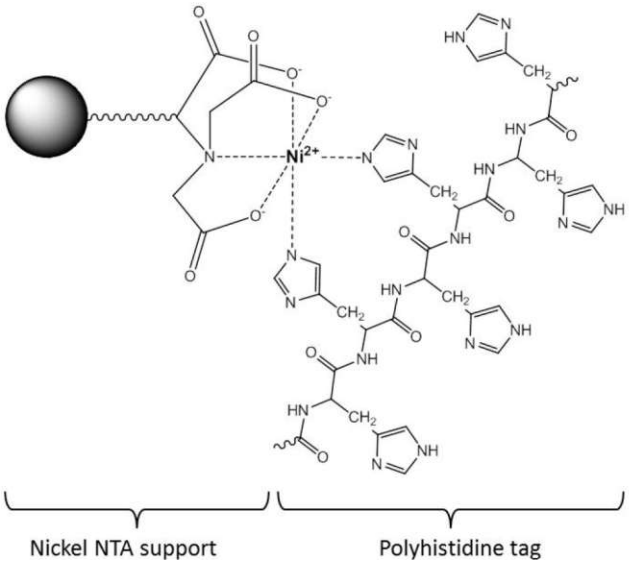

Figure 2.3.: Complex formation of a poly-His tag with Ni-NTA. [41]

2.2.2. His-tag binding to Ni-chelated lipids

Several studies have been conducted concerning the association and dissociation behaviour of His-tagged proteins to Ni-NTA. Like mentioned above, His-tags bind to the Ni^{2+} ions through their side chains; two imidazole side-chains of individual His residues are supposed to bind to a single Ni-NTA (Figure 2.3). [17] This proposed binding mode was confirmed by Kirk et al. [42], as they studied imidazole-ligand binding to Ni-NTA in titration calorimetry measurements. Their results indicate, that the binding of one imidazole group leads to a conformational change in the Ni-NTA, which opens a second binding site. Similarly, Nye et al. [18] proposed that the adsorption process occurs in two-steps: First, free protein binds monovalently to the Ni-chelated lipids through a single His residue. Afterwards, the adsorbed species are supposed to bind further lipids through other His residues to form a stable, polyvalently bound protein-lipid complex. Whether the binding occurs to one or more lipids remains uncertain. In general, these findings show that more than one imidazole-group and ergo more than one His residue is necessary for stable association.

Concerning protein desorption, Nye et al. [18] likewise suggested a two-step process, including a rather long transition from polyvalently to monovalently bound proteins, followed by quick desorption of monovalently bound proteins from the surface. They studied the unbinding of GFP tagged with 10 His residues (H10-GFP) from a SLB over 23 hours (Figure 2.4). After two hours only about 40% of H10-GFP remained on the bilayer, but the residual amount showed slow desorption

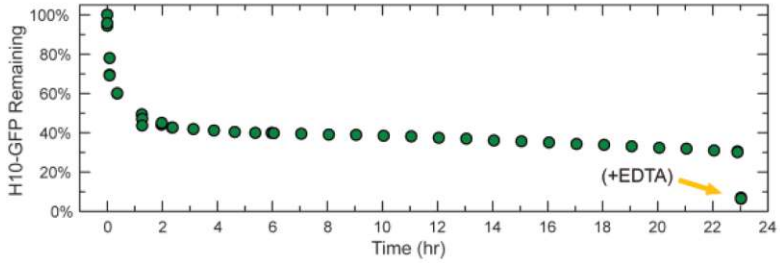

Figure 2.4.: Unbinding of His-tagged GFP over 23 hours observed by Nye et al. [18]

over the subsequent period. The last data point was recorded after washing with EDTA to measure unspecific binding, since only proteins remain which are not bound through the Ni-His interaction. The desorption rate constant was determined as $9.8 \cdot 10^{-4}$ min^{-1}. Furthermore, Nye et al. observed, that surface binding sites are quickly saturated at high protein concentrations, thereby preventing the formation of stable polyvalent complexes. However, this can be avoided by incubating at intermediate protein concentrations for prolonged time, which allows the transition from monovalent to polyvalent binding. [18]

To the best of one's knowledge only one other group studied the desorption of His-tagged proteins, although not on SLBs but on liposomes, over such a long period. Platt et al. [22] used monomeric Katushka (mKate) tagged with six His residues and observed similar dissociation behaviour. After approximately three hours only 40% of mKate were retained on liposomes; this value decreased further to around 20% after 24 hours.

2.2.3. Influences on the binding stability

There are other factors which influence the binding stability, such as the number of His residues and His-tags. Although both of these factors have not been investigated on SLBs, their effect has been studied with surface plasmon resonance (SPR).

Knecht et al. [19] examined the interaction of His-tags with various residues (ranging from dihistidine to decahistidine) with Ni-NTA. Their measurements showed that increasing the number of residues leads to slower dissociation and higher stability (Figure 2.5a). Concerning the binding affinity, the association constant K_A was highest for six His residues (Figure 2.5b). Shorter peptides (di-, tri-, tetrahisitidine) exhibit rather low affinity compared to tags with intermediate length (penta-, hexa-, hepta-, octahistidine). For longer peptides (penta-, decahistidine) the affinity dropped again. This behaviour can be explained by thermodynamic means with the Gibbs free energy ($\Delta G = \Delta H - T\Delta S$). When the number of residues rises, the probability of coordination bonds and rebinding events increases, thus increasing the enthalpy term ΔH. However, above a certain

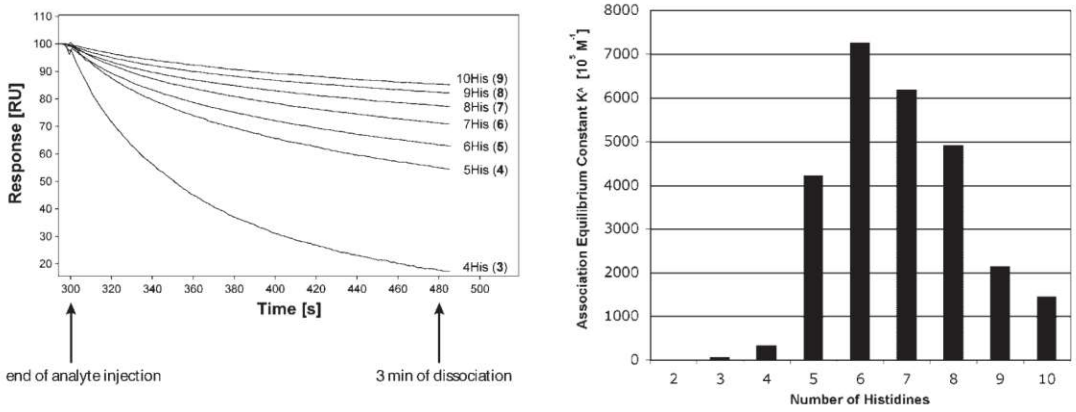

(a) (b)

Figure 2.5.: Results of SPR measurements for tags with a different number of His residues. a) Normalised plots of the dissociation phase. With increasing number of His residues, dissociation is slower and binding is more stable. b) Association constant K_A of oligohistidines. Hexhistidine has the highest binding affinity, above and below the affinity drops. [19]

length, the conformational freedom increases disproportionately and the entropy term $T\Delta S$ outbalances the enthalpy contribution. Due to this, hexahistidine has the optimal length and offers a balance between the gain in enthalpy and the cost in entropy.

The effect of the number of His-tags on the binding to Ni-NTA has been studied by Nieba et al. [20] also with SPR. Each His-tag included a sequence of six His residues. For the protein GroES with five to six His-tags (Figure 2.6a, curve 1) as well as for the protein citrate synthase with two His-tags on each terminus (Figure 2.6a, curve 2) no dissociation was detected. Citrate synthase with only two His-tags on the C terminus did not bind stably (Figure 2.6a, curve 3), but the protein GrpE with two His-tags (Figure 2.6a, curve 4) showed no dissociation. Finally, maltose-binding protein with a C-terminal His-tag (Figure 2.6a, curve 5 and Figure 2.6b, curve 3) dissociated rapidly from the surface. The same behaviour was also observed when the tag was placed on the N terminus (Figure 2.6b, curve 2), but labelling both C and N terminus with a His-tag, led to stable binding (Figure 2.6b, curve 1). Consequently, using an increased number of His-tags and taking advantage of the avidity effect by simultaneous binding with two tags to the Ni-NTA increases the binding stability.

Another way to improve the binding is by using trisNTA, a complex of three Ni-NTA groups. Compared to monovalent NTA, such multidentate chelator headgroups led to decreased dissociation rates of complexes formed with oligohis-

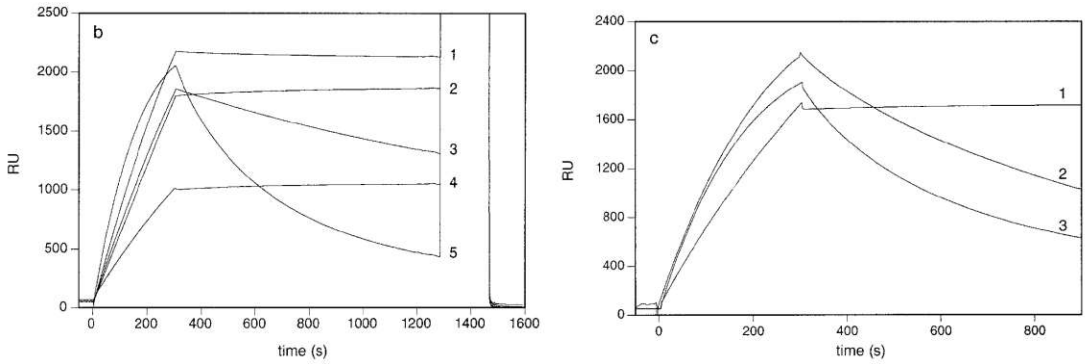

(a) (b)

Figure 2.6.: Results of SPR measurements of proteins with a different number of His-tags. a) Plots of GroEs with five to six His-tags (curve 1), citrate synthase with four His-tags (curve 2), citrate synthase with two His-tags (curve 3), GrpE with two His-tags (curve 4) and maltose-binding protein with a C-terminal His-tag (curve 5). b) Plots of maltose-binding protein with a His-tag on both N and C terminus (curve 1), only on the N terminus (curve 2) and only on the C terminus (curve 3). [20]

tidines [21] and a higher percentage of His-tagged proteins remained bound over several hours to trisNTA containing liposomes [22]. However, not many lipids are commercially available in conjugation to trisNTA, due to a rather complex synthesis and high cost of free trisNTA. Due to this, Xiao et al. [43] fabricated a library of NTA conjugated Janus dendrimers (JDs). JDs are synthetic lipids, which can be used as biological membrane mimics. The research group did not only observe stable binding of His-tagged GFP to liposomes containing JD-NTA, but the binding affinity was even higher compared to commercially available DGS-NTA and increased further for liposomes containing JD-trisNTA. How JDs with trisNTA affect the binding of His-tags on SLBs remains an intriguing question that still needs to be resolved.

2.3. T cell activation

Like mentioned above, SLBs are used in a broad range of applications, for instance to study the activation of T cells [31]. T cells are lymphocytes and play a crucial part in cell-mediated immunity. Generally, lymphocytes are able to react to a vast number of microbial substances, called antigens. They recognise precise differences in the epitopes of antigens, leading to great specificity in re-

sponse. To detect such antigens, T lymphocytes have a specific antigen receptor, called T cell receptor (TCR). TCRs recognise peptide fragments on the surface of antigen-presenting cells (APCs), but only when they are bound to MHC molecules. [3] MHC molecules are cell surface glycoproteins that can be differentiated into class I and class II molecules. Class I molecules present antigens mainly to $CD8^+$ cytotoxic T lymphocytes, which recognise and eliminate virus-infected cells, and class II molecules bind antigens primarily recognised by $CD4^+$ helper T cells, that regulate cellular and humoral immune functions by secreting cytokines. [4] For this thesis only class II molecules are of interest. However, since they share similar structural features, both will be briefly explained.

Class I MHC molecules (Figure 2.7a) consist of a transmembrane α chain which is non-covalently associated with a smaller subunit, termed β_2-microglobulin. The binding of antigen is mediated by the α_1 and α_2 domain of the α chain. They are each composed of one α helix and four β strands. When the two subunits associate, the α helices form a grove on the β strand platform, where the antigen can bind. [44, 45]

Class II MHC molecules (Figure 2.7b) show similarities to class I molecules in the overall structure. However, they consists of two transmembrane, non-covalently attached polypeptide chains, termed α and β chains. Both have two extracellular domains (α_1, α_2 and β_1, β_2 respectively for the α and β chain), a transmembrane domain and an intracellular domain. The binding grove is formed by the membrane-distal α_1 and β_1 domains and consists similarly to class I molecules of eight β sheets and two α helices; the membrane-proximal domains α_2 and β_2 provide support for the formed binding grove. [44–46]

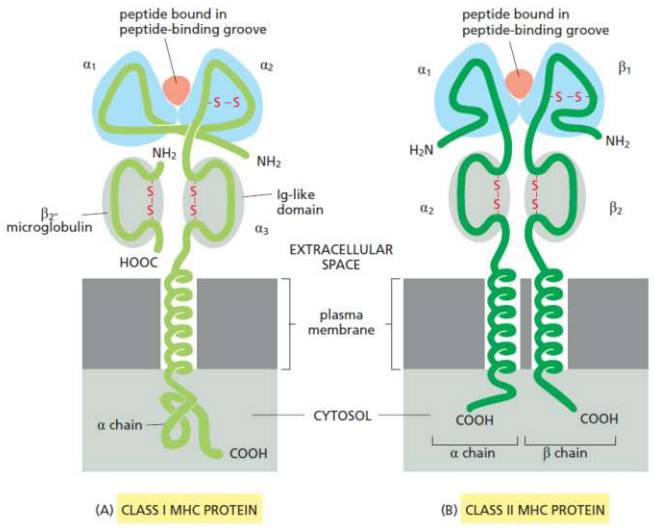

Figure 2.7.: Sketch of MHC class I (A) and class II (B) molecules. [2]

The binding of TCR to the antigen-MHC-complex initiates T cell activation. Consequently, among other molecules necessary for cell adhesion, MHC molecules need to be present on bilayers to achieve activation. [4]

While fever is a typical response to infection or inflammation, its precise effect is still not fully understood. In general, the rise in body temperature is associated with enhanced organism survival and improved effectiveness of the immune system by stimulating both innate and adaptive immune responses. [5] The effect of temperature on lymphocytes in particular is still a topic of ongoing research. Studies have shown that fever-range thermal stress enhances the ability of lymphocytes to respond to stimulatory signals. In cytotoxic T cells, pre-association of TCR and CD8 was observed, which prolongs stable contact with APCs. [6, 7] Furthermore, febrile temperatures reduce the need for co-stimulating molecules of helper T cells. Activation is easier and more quickly under these conditions. [8] Another mechanism which is triggered by fever-range temperatures is the heat shock protein 90 (Hsp90)-α4-integrin pathway. Thermal stress induces upregulated expression of Hsp90 and promotes binding to α4 integrins, which in turn increases α4 triggered T cell adhesion and transmigration. [9]

To sum up, the activation of T lymphocytes under physiological and febrile temperatures is still a topic of ongoing research and can be studied with SLBs. Therefore, peptide-major histocompatibility complex (pMHC) molecules need to be present on the bilayer, which are bound through His-tags to Ni-chelated lipids. Consequently, stable protein binding and bilayer quality are of fundamental importance. Since the effect of physiological temperatures on the stability of SLBs as well as on the binding of His-tagged proteins has not been investigated so far, gaining more insight may help to improve experimental conditions involving His-tagged proteins.

3. Material and Methods

The general protocol was identical for all experiments. Functionalised SLBs were prepared in a Nunc™ Lab-Tek chamber (LTC) (Thermo Scientific™). Since the stability depending on the number of His tags at ambient temperature (21°C) and physiological temperature (37°C) was of interest, four different protein probes were utilised. In each experiment, bilayers were functionalised with only one protein and imaging was performed at either of the named temperature conditions over several hours using single molecule fluorescence microscopy. Furthermore, two different approaches were tested to improve the binding stability of one protein at 37°C. In one experiment, potential free binding sites were recharged by incubating bilayers with Nickel(II)-chlorid ($NiCl_2$) before protein functionalisation, since it is possible that Ni^{2+} ions dissociate from the NTA adsorbent. In the other experiment, the pH of the buffer was increased, which leads to deprotonation of the His residues and potentially to improved binding stability.

3.1. Proteins

The behaviour of the protein IE^K was of interest, because it acts as the respective antigen to the TCR of 5cc7 helper T cells; the crystal structure can be seen in Figure 3.1. IE^K is a pMHC molecule with two His tags and six His residues, which was specifically labelled with Alexa Fluor 647 (AF647). It is stored with a concentration of $c = 64$ ng/µl in solution (50% 1xDPBS and 50% glycerol).

The other proteins utilised for this study were three different versions of Streptavidin. Streptavidin is a homotetramer with a molecular weight of approximately 56 kDa and high thermostability. It can bind up to four biotin molecules with high affinity. [47] Biotin-binding subunits are termed alive, whereas other non-binding subunits are termed dead. For this thesis, monovalent Streptavidin (mSAV), divalent Streptavidin (diSAV) and trivalent Streptavidin (triSAV) were prepared. A schematic of each type can be seen in Figure 3.2. Monovalent Streptavidin-biotin-AF647 (Figure 3.2c) has one alive subunit and three dead subunits, which each has a His tag of six residues. Divalent Streptavidin-biotin-AF647 (Figure 3.2b) has two biotin-binding subunits and two His tags, each bound to one dead subunit. Trivalent Streptavidin-cystein-AF647 (Figure 3.2a) has three alive subunits with cystein bound instead of biotin and one His tag on the dead subunit.

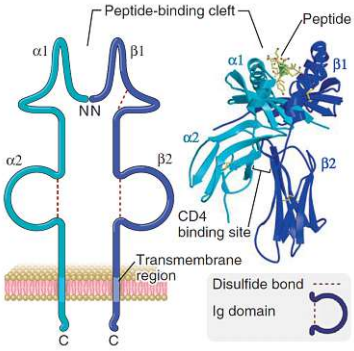

Figure 3.1.: Schematic (left) and crystal structure of the extracellular domain (right) of a class II pMHC molecule acting as antigen to TCR of 5cc7 helper T cells. [3]

All types of Streptavidin were labelled with AF647; the fluorophore was attached to the alive subunit either by binding biotin (mSAV, diSAV) or cystein (triSAV). All three version were stored in solution (50% 1xDPBS and 50% glycerol) at concentrations of $c = 160$ ng/µl, $c = 100$ ng/µl and $c = 550$ ng/µl, respectively for mSAV, diSAV and triSAV.

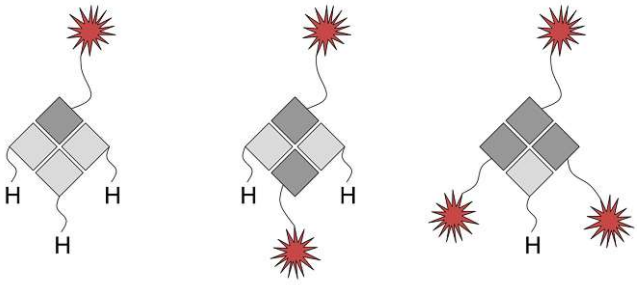

(a) (b) (c)

Figure 3.2.: Schematic of the three different types of Streptavidin used: a) mSAV, b) diSAV, c) triSAV. The His tag (H) was attached to the dead subunit (light grey) and the fluorophore was either bound to biotin in case of mSAV and diSAV or cystein for triSAV on the alive subunit (dark grey).

All proteins were obtained due to a collaboration with Johannes B. Huppa from the Institute for Hygiene and Applied Immunology at the Medical University of Vienna. The peptides were fabricated by René Platzer. The preparation process can be found in detail for example in [48] and [49].

3.2. Bilayer Preparation

3.2.1. Lipid Vesicles

First, the vesicle solution was prepared using 1-palmitoyl-2-oleoyl-glycero-3-phosphocholine (POPC) (Avanti® Polar Lipids, Inc.) and 1,2-dioleoyl-sn-glycero-3-[(N-(5-amino-1-carboxypentyl)iminodiacetic acid)succinyl] (nickel salt) (DGS-NTA(Ni)) (Avanti® Polar Lipids, Inc.). Both lipids were purchased as powder and dissolved in chloroform to obtain stock solutions with concentrations of 10 mg/ml POPC and 1 mg/ml DGS-NTA(Ni). The lipids were mixed in a composition of 98% POPC and 2% DGS-NTA(Ni) with a concentration of 125 µM. In four experiments, 1,2-dioleoyl-sn-glycero-3-phosphoethanolamine (DOPE)-Atto488 was added at a ratio of 1 : 100000, i.e. 1 DOPE-Atto488 molecule per 100000 other lipid molecules, to observe the behaviour of the bilayer itself. DOPE fluorescently labelled with Atto488, was provided by Radek Šachl from the J. Heyrovsky Institute of Physical Chemistry of the Czech Academy of Sciences. The lipid was previously diluted in a solvent of two parts chloroform and one part methanol to a concentration of $7.5 \cdot 10^{-9}$ mol/l. After mixing all lipids in a glass vial, the chloroform was evaporated with nitrogen for 20 min, 1 ml $10x$ DPBS (Sigma-Aldrich®) was added and the solution was mixed on a Vortex mixer (IKA Labortechnik). Afterwards, vesicles were formed by sonication for 15 min at room temperature in an Ultrasonic cleaner (VWR™).

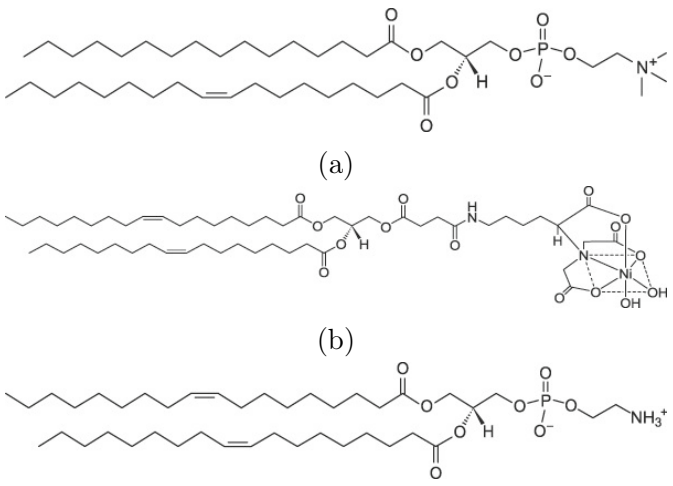

Figure 3.3.: Chemical structures of lipids used for vesicle preparation: a) POPC [50], b) DGS-NTA(Ni) [51], c) DOPE [52].

3.2.2. Bilayer Functionalisation

The SLBs were prepared in a LTC on a glass cover slip. The cover slips were cleaned using a Plasma Cleaner (Harrick Plasma) for at least 15 min and fixated on the LTCs with eco-sil extrahart Addition-curing duplicating silicone (picodent®). 200 µl of the vesicle solution was added to each well and incubated for 20 min at room temperature. Afterwards, each well was washed with 25 ml $1x$ DPBS (Sigma-Aldrich®), the meniscus and 330 µl were removed, so that 450 µl remained in each well. In final experiments recharging of potential free NTA sites was tried to improve the binding stability of IE^K. Nickel(II)-chlorid was prepared in 1x DPBS buffer at a concentration of 1 M. 50 µl were added to the washed bilayers, so that a final concentration of 100 mM was obtained. The bilayers were incubated for 5 min and the washing process was repeated afterwards.

For all experiments two different dilutions of each protein, namely one with high and low protein incubation concentration were prepared by mixing the protein solution with $1x$ DPBS. Bilayers incubated with high protein concentration mimic positive controls of T cell experiments and bilayers with low incubation concentration were used to determine the single molecule brightness. For IE^K two experiments were performed at 21°C, yielding a total of four bilayers with high and two bilayers with low incubation concentration. For all other experiments always three bilayers were prepared with high protein incubation concentration and one bilayer was fabricated with low incubation concentration. It has to be noted, that bilayers functionalised with mSAV were prepared with slightly lower incubation concentration for the experiment at 37°C, since rather high brightness values were observed in the experiment at 21°C, that could probably lead to issues with the camera saturation. 50 µl of each dilution were added to the 450 µl $1x$ DPBS contained in each well. The final protein incubation concentrations can be found in Table 3.1. After adding the proteins, the LTCs were again incubated at room temperature for 60 min, washed with 25 ml 1x DPBS and finally the DPBS was exchanged with HBSS (Sigma-Aldrich®).

For the second approach to improve the binding stability HBSS with pH = 8 and pH = 8.5 were prepared by dropwise adding 1 M sodium hydroxide (NaOH) while constantly measuring the pH of the solution at room temperature. In this experiment three bilayers were incubated with high IE^K concentration, washed with 1x DPBS and the DPBS was exchanged once with unchanged HBSS, once with pH = 8 HBSS and once with pH = 8.5 HBSS.

Table 3.1.: Final incubation concentrations of proteins in different experiments.

Protein	Temperature	High incubation concentration [ng/ml]	Low incubation concentration [ng/ml]
IE^K	21°C	20	0.4
	37°C	20	0.4
triSAV	21°C	200	2
	37°C	200	2
diSAV	21°C	60	0.6
	37°C	60	0.6
mSAV	21°C	80	0.8
	37°C	60	0.6

3.3. TIRF Microscopy Imaging

All data were acquired with a Total Internal Reflection Fluorescence (TIRF) Microscope. For the excitation of the fluorescently labelled proteins a red laser with a wavelength of $\lambda = 642$ nm was used with a power of 120 mW and 95% of 3.5 mA current. The fluorescently labelled lipids were excited with a blue laser at $\lambda = 488$ nm of 150 mW power and 95% of 0.1 mA current. The laser settings were adjusted with the software *Oxxius Lasers*. As dichroic mirror the filter FITC/Cy5 was chosen and as emission filter the 538/685 HC Dualband Filter (FITC/Cy5) (Semrock) was used. For imaging, a 100x apochromat objective (Carl Zeiss Microscopy) was used and the tube lens had a 1x magnification. The images were acquired with an iXon EMCCD camera (Oxford Instruments) in two colour mode. Therefore, an Optosplit II image splitter (Oxford Instruments) was used to divide the image into two separate components. In the channel for the red laser the filter HQ700/75m (Chroma®) was mounted and in the channel for the blue laser the single band pass 525/45 BrightLine HC (Semrock) was inserted to select the emission wavelength of fluorophores with which the lipids were labelled.

The setup was operated with the LabVIEW program *SDT-Control*. The correct lasers were selected and the imaging parameters were adjusted: 100 image frames were acquired with an illumination time of 5 ms and a delay of 20 ms. Furthermore, the laser power was reduced to 30% of the maximum laser intensity. The TIRF position could be adjusted with the LabVIEW program *Servotisch*. The best possible TIRF position was individually adapted on each day.

Before placing the LTC in the sample holder, an immersion oil (Carl Zeiss™ Immersol™ 518 F) was applied on the objective and the LTC was cleaned with ethanol. Five image sequences were acquired of the fluorescently labelled proteins using the red laser and the respective camera channel. In experiments where the

tracer lipid DOPE-Atto488 was added, the blue laser was operated simultaneously and five image sequences were acquired in two colour mode, where the red and blue channel are displayed on the same image. However, bilayers with low protein incubation concentration were always imaged without the blue laser. Prior to each acquisition the sample position was changed and the focus was optimised.

This imaging process was conducted for each bilayer over the course of three to five hours so that protein surface density values could be determined at different time points. Imaging was performed at two different temperature conditions, namely around 21°C and 37°C. For the latter the chamber around the microscope was heated up to 40°C with the temperature control unit Tempcontrol 37-2 digital (PeCon®). Furthermore, an objective heating ring was mounted and operated at 40°C with the Tempcontrol mini (PeCon®) temperature control unit. During experiments performed at higher temperature, the temperature inside the wells of the LTC was periodically measured. Depending on the contact duration of the objective heating with the cover slip below each well, the temperature varied between $36-38$°C, and is thus further denoted as 37°C. In some of the experiments 50 µl of 1 M in H_2O imidazole buffer solution (Sigma-Aldrich®) was added in the end. This step was included to test the specificity of binding, since imidazole is a competing electron donor and replaces the His tag.

3.4. Data analysis

To assess the behaviour of functionalised SLBs at different temperatures over time, the acquired images were first qualitatively evaluated regarding protein mobility and brightness. Since considerable differences could even be observed in the raw data, quantitative analysis was conducted to get more detailed results. Therefore, a pre-existing Python-based brightness analysis algorithm (provided by Caroline Kopittke) was used and slightly adapted with Jupyter notebook. Surface density values were determined over time and a desorption model was fitted based on simple binding kinetics. An overview of the individual steps of the data analysis for each experiment is given in a flow chart in Figure 3.4.

3.4.1. Region-of-interest selection

As first step of the analysis, the region-of-interest (ROI) as well as the region for the background correction had to be determined. The ROIs were carefully selected, since only signals and intensity values in the center of the Gaussian laser profile are reliable. Due to this, 80x80 pixel regions were manually defined with ImageJ and the area A_{ROI} was calculated in Python, corresponding to 12.8x12.8 μm^2.

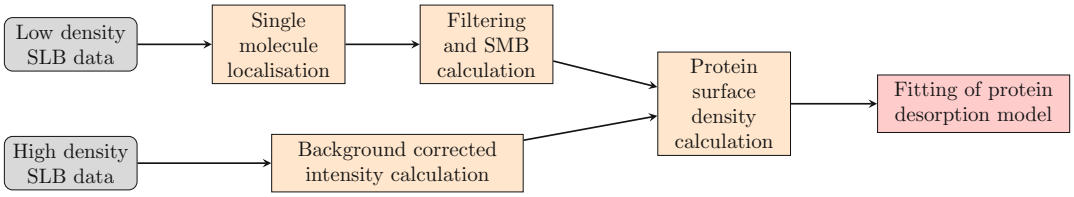

Figure 3.4.: Overview of the individual steps of the data analysis visualised in a flow chart.

3.4.2. Single Molecule Brightness Determination

In order to calculate the protein surface density, the single molecule brightness (SMB) needs to be known. Therefore, single molecules on microscopy images of bilayers with low protein incubation concentration were localised first with the fluorescent feature localisation GUI of the sdt-python package by Lukas Schrangl [53]. It provides an implementation of the 3D-DAOSTORM algorithm (for more detail please refer to [54]). First, a brightness threshold needs to be set; only signals above this threshold are considered for fitting of a 2D Gaussian with variable size. The software extracts several features of each found localisation, like the position (x- and y-coordinates as well as the frame number), the size (given by the standard deviation) and the amplitude of the Gaussian curve as well as the local background and integrated intensity corrected by the background. The features are stored in a dataframe and further used for diffusion analysis to exclude immobile molecules. Therefore, particles are tracked with Trackpy v0.5.0 [55] using a tracking radius of 3 px and a minimum tracking length of 3 image frames. Afterwards, the diffusion coefficient is determined with the diffusion analysis module of the sdt-python package [53], which calculates the mean-squared displacement of molecules and determines the diffusion coefficient assuming Brownian motion. For further analysis only molecules equal to or above $D = 0.03\ \mu m^2/s$ are considered.

Another aspect which needs to be regarded are false positive localisations. When the density is too high, some molecules come into contact and are probably recognised as a single localisations. Such signals could falsify the mean SMB and thus the found localisations are further filtered. Concerning proteins which are only labelled with one fluorophore (IE^K and mSAV) localisations on the first few image frames are disregarded due to the named reason of possible false positive localisations. In later frames the density is lower and consequently also the probability of false positive localisations. For these two proteins frame 10 was chosen as starting frame for the SMB determination. However, the other two proteins (diSAV and triSAV) are labelled with more than one fluorophore and choosing signals on later frames could lead to distorted brightness values due to photobleaching.

Consequently, the density on these bilayers was kept rather low to reduce the probability of random encounters and thus localisations on the first image frame could be used for the calculation.

Before determining the mean SMB additional filtering by intensity, local background and size was performed to further reduce the possibility of including non-monomeric localisation. Such data points would probably be visible as outliers in the single molecule intensity and background distributions and are thus excluded. Concerning the size of found localisations, only signals within the main part of the size distribution were considered, since large fit sizes could possibly be caused by overlapping fluorophores that are fitted with a larger Gaussian and small fit sizes could arise for example due to camera noise.

After filtering the SMB data the mean intensity I_{SMB} [counts/signal] of all remaining localisations was determined and further used for the calculation of protein surface densities.

3.4.3. Protein Surface Density Calculation

To determine the protein surface density, the background corrected intensity I_{corr} within in the ROI of the first image frame was calculated first. Therefore the mean background intensity $I_{\mathrm{background}}$ was subtracted from the mean intensity I_{raw} within the ROI

$$I_{\mathrm{corr}} \left[\frac{\mathrm{counts}}{\mathrm{px}}\right] = I_{\mathrm{raw}} - I_{\mathrm{background}}. \tag{3.1}$$

The protein surface density ρ was then determined by dividing the background corrected intensity I_{corr} by the SMB I_{SMB} and the pixel size

$$\rho \left[\frac{\mathrm{signals}}{\mu\mathrm{m}^2}\right] = \frac{I_{\mathrm{corr}} \left[\frac{\mathrm{counts}}{\mathrm{px}}\right]}{I_{\mathrm{SMB}} \left[\frac{\mathrm{counts}}{\mathrm{signal}}\right] \cdot 0.16^2 \left[\frac{\mu\mathrm{m}^2}{\mathrm{px}}\right]}. \tag{3.2}$$

3.4.4. Desorption model

For each bilayer surface density values were calculated and plotted over time. To explain the dissociation behaviour a desorption model was developed based on simple receptor-ligand kinetics of a single receptor and a single ligand. Model fitting was performed with the *optimize.curve_fit* function of the SciPy package in Python 3.9.4. After calculating the fitting variables, the functions were normalised to the initial starting value of the fits at t_0 for better comparison. As start t_0 the timepoint was chosen when the final washing process of the bilayers was finished. Moreover, for each experiment the mean and standard deviation (sd) of the off-rates were calculated.

3.4.5. Bilayer stability and lipid detachment

To determine the effect of the temperature on the bilayer itself, images of the tracer lipid DOPE-Atto488 were first qualitatively and then quantitatively evaluated. For quantitative analysis, the bulk brightness of the tracer lipids within the ROI was determined over time analogously to Equation 3.1. The decrease in brightness was modelled with an exponential function

$$I = I_0 \cdot e^{-k_{off} \cdot t} \tag{3.3}$$

and normalised by the initial value of the fit $I(t_0)$

$$I_{\text{norm}} = \frac{I}{I(t_0)}. \tag{3.4}$$

t_0 corresponds again to the timepoint when the final washing process was finished. Furthermore, the mean and sd of the off-rates were calculated.

4. Results

To asses the stability of functionalised SLBs the behaviour of the lipid bilayer itself is first analysed regarding the persistance against lipid detachment and hole formation in section 4.1. Next, a desorption model is developed in section 4.2 to explain the observed dissociation behaviour of proteins by means of simple receptor-ligand-kinetics. In the following subsections 4.2.1-4.2.4, always three raw data images of a bilayer functionalised with a specific protein and incubated at 21°C and 37°C are qualitatively analysed. Furthermore, the developed model is applied to the calculated protein surface density values and mean off-rates are determined. In the end, two approaches were tested to improve the binding stability. One approach was to recharge potential free NTA binding sites by incubating bilayers with $NiCl_2$ (section 4.3) and the other approach included varying the pH of the HBSS buffer (section 4.4).

4.1. Bilayer stability and lipid detachment

First, the behaviour of the lipid bilayer at 21°C and 37°C was studied over time. Therefore, the fluorescently labelled lipid DOPE-Atto488 was include in the vesicle composition. Qualitative assessment of the raw data showed that the bilayers remain mobile and largely adhere to the cover slip over the course of the experiments for both temperature conditions. Three exemplary raw images of one bilayer at different timepoints during experiments performed at 21°C and 37°C are provided in Figure 4.1 and Figure 4.2, respectively. For room temperature conditions no obvious lipid detachment could be observed, whereas in case of elevated temperature conditions some bilayers showed the formation of small holes over the course of the experiments and also slight reduction in overall brightness. However, in preliminary experiments (data not included) minor holes could also be observed for room temperature conditions.

To quantify these observations, the background corrected bulk brightness within the ROI of the first image frame was determined as a function of time (Figure 4.3). An exponential model without vertical offset was fitted to the data according to Equation 3.3. Afterwards, the exponential functions were normalised to the fit value of t_0 according to Equation 3.4 for better comparison (Figure 4.4). Apart from statistical fluctuations in the data, bilayers showed no decrease in mean

brightness when the experiments were performed at room temperature. The mean ± sd off all fitted off-rates resulted in $k_{off,\ 21°C} = (2.8 \pm 3.9) \cdot 10^{-5}$ min^{-1}. In comparison to that, increasing the temperature to approximately 37°C led to a higher decrease in observed mean brightness, with an off-rate of $k_{off,\ 37°C} = (1.1 \pm 0.3) \cdot 10^{-3}$ min^{-1}, that represents the mean ± sd of all fitted off-rates. Resulting values of the exponential fits can be found in Appendix A.

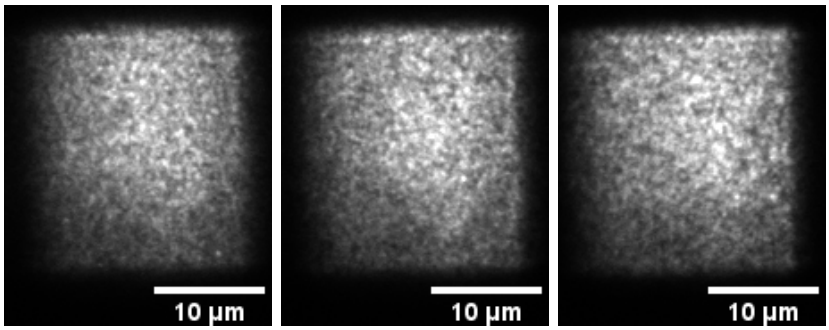

(a) (b) (c)

Figure 4.1.: Bulk brightness of the tracer lipid DOPE-Atto488 at approximately 21°C over the course of several hours. The first image frame of an acquisition is shown at a) $t = 9$ min, b) $t = 128$ min, c) $t = 285$ min after the washing process of the bilayers was finished. All images have equal brightness scales.

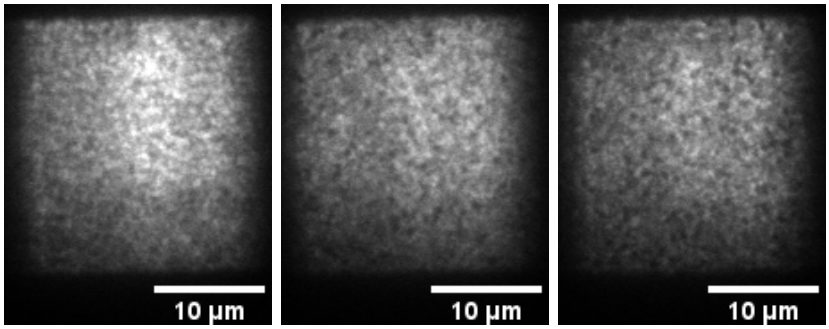

(a) (b) (c)

Figure 4.2.: Bulk brightness of the tracer lipid DOPE-Atto488 at approximately 37°C over the course of several hours. The first image frame of an acquisition is shown at a) $t = 27$ min, b) $t = 136$ min, c) $t = 249$ min after the washing process of the bilayers was finished. All images have equal brightness scales.

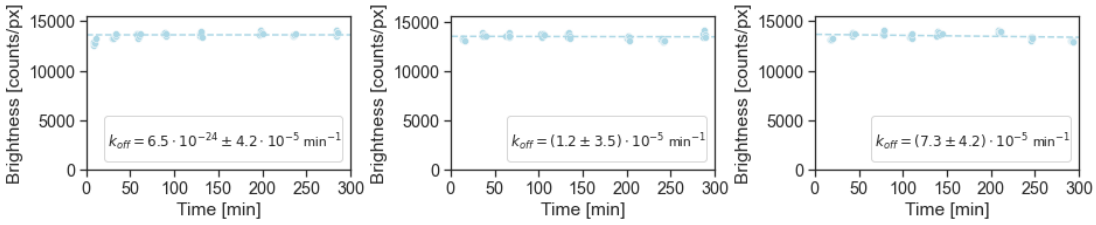

(a)

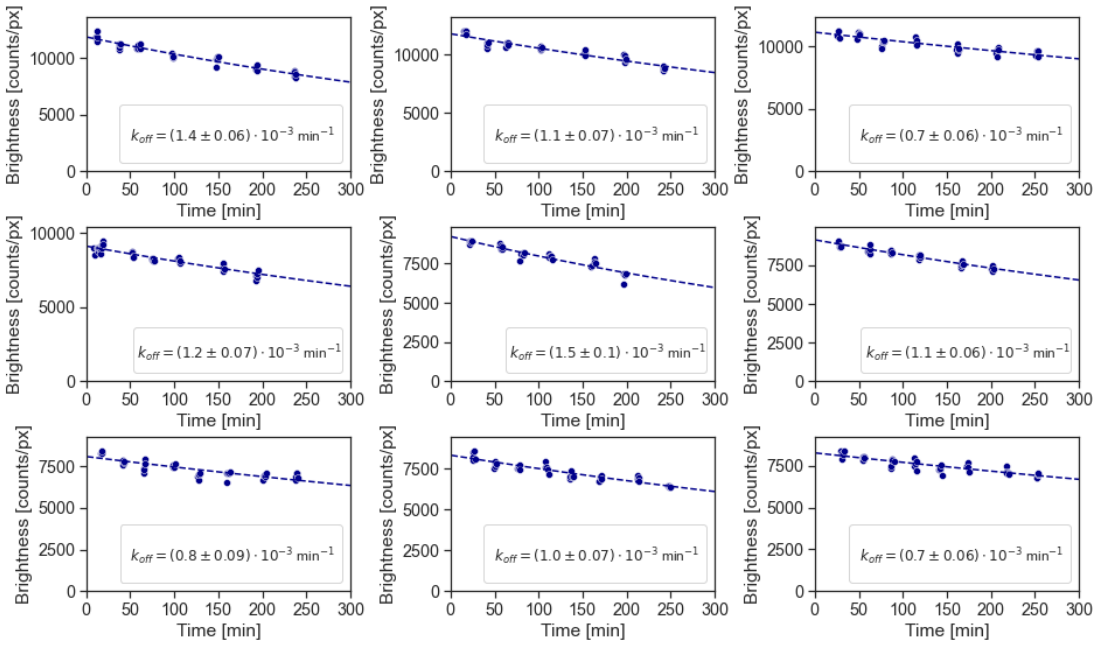

(b)

Figure 4.3.: Decrease in bulk brightness of the tracer lipid DOPE-Atto488 in experiments at a) 21°C and b) 37°C. Each plot shows the resulting intensity values of one bilayer including exponential fits and fitted off-rate. Plots in one row correspond to data of bilayers imaged in the same experiment.

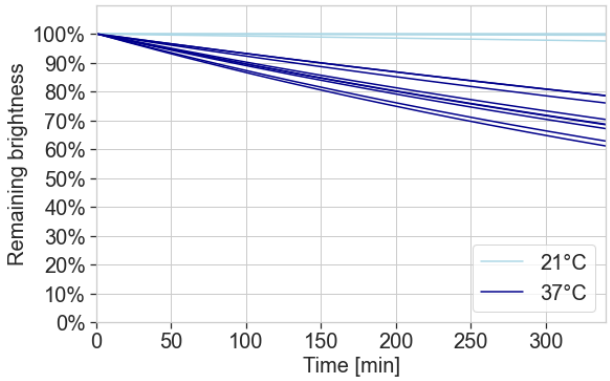

Figure 4.4.: Normalised exponential fits of the decrease in bulk brightness of the tracer lipid DOPE-Atto488. Off-rates (mean ± sd) were $k_{off,\ 21°C} = (2.8 \pm 3.9) \cdot 10^{-5}$ min^{-1} and $k_{off,\ 37°C} = (1.1 \pm 0.3) \cdot 10^{-3}$ min^{-1} respectively for bilayers imaged at 21°C and 37°C.

4.2. Modelling protein desorption

To determine the stability of protein-functionalised SLBs at two different temperature conditions, TIRF images of bilayers were first qualitatively analysed. To explain the observed behaviour, a desorption model was developed based on simple receptor-ligand-kinetics. Therefore, protein surface densities were determined over time (Equation 3.2). To calculate density values, the mean brightness of single molecules was determined after localisation and filtering; resulting SMB values including the settings for filtering can be found in Appendix B.

Based on the observed behaviour, a one-step desorption process is proposed. Protein unbinding is modelled by a standard first order rate equation:

$$\frac{\mathrm{d[RL]}}{\mathrm{d}t} = k_{on}[\mathrm{R}][\mathrm{L}] - k_{off}[\mathrm{RL}] \tag{4.1}$$

[RL] represents the protein bound through the His-tag to the Ni-NTA, [R] the receptor, i.e. the Ni-NTA and [L] the ligand, i.e. unbound protein. A simple schematic is visible in Figure 4.5. The first term of the rate equation including the on-rate k_{on} describes the binding of free protein via the His-tag the Ni-NTA, whereas the second term including the off-rate k_{off} describes the unbinding of protein from the bilayer.

For this thesis only the desorption of proteins was of interest. In the beginning of the experiments no unbound protein is present in the solution. Over time, proteins

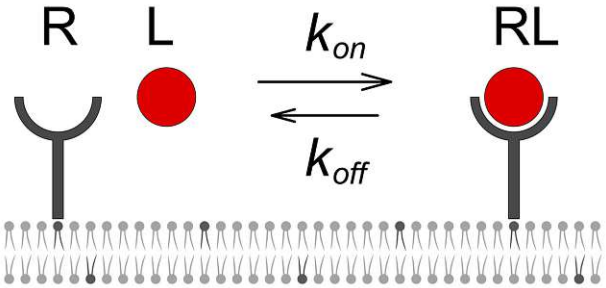

Figure 4.5.: Schematic of receptor-ligand interaction with a single receptor and a single ligand which form a complex. R represents the Ni ions on the DGS-NTA substrate, L the His-tag and RL the formed complex. POPC (light grey) and DGS-NTA(Ni) (dark grey) lipid ratio displayed is not in proportion to real vesicle composition (98% POPC and 2% DGS-NTA(Ni)).

dissolve from the bilayer. Since the surrounding volume is large compared to the amount of contained dissociated proteins, the probability of rebinding is expected to be very low and thus, the binding term is assumed to be zero ($k_{on}[\mathrm{R}][\mathrm{L}] = 0$). The remaining part of the rate equation

$$\frac{\mathrm{d}[\mathrm{RL}]}{\mathrm{d}t} = -k_{off}[\mathrm{RL}] \tag{4.2}$$

can be solved by an exponentially decaying function

$$\mathrm{RL}(t) = \mathrm{RL}_0 \cdot e^{-k_{off} \cdot t} + \mathrm{RL}_{\mathrm{const}}. \tag{4.3}$$

Equation 4.3 models the decrease in protein surface density ρ, where RL_0 represents the initial surface density at t_0 and k_{off} the off-rate. t_0 corresponds to the time when the washing process of the bilayers was finished. The offset $\mathrm{RL}_{\mathrm{const}}$ is an optional term and fitted depending on the observations in the raw data. If most of the proteins aggregated and immobile clusters were detected over time, the fitted function contained an offset. If bilayers remained mobile over the course of the observed period, the offset was not included.

4.2.1. IE^K

The developed desorption model was first applied to protein surface density values of bilayers functionalised with IE^K. IE^K is a pMHC molecule that acts as the respective antigen to the TCR of 5cc7 helper T cells. It has two His-tags, each with six His residues. In experiments where imaging was performed at room temperature (21°C) the behaviour of four funtionalised bilayers was observed over nearly 5 hours with single molecule microscopy. Exemplary TIRF images of a bilayer at three different points in time during one experiment are visible in Figure 4.6. The raw data showed, that the proteins remained mobile on all bilayers and only in one case a very small fraction of immobile molecules was visible. However, a decrease in surface density could even be observed in the raw data, since the overall brightness decreased.

Compared to that, the behaviour of IE^K changed drastically when the bilayer temperature was increased to 37°C. Raw data images of one bilayer at three points in time can be seen in Figure 4.7. At the beginning of the experiment the pMHC molecules were mobile on all bilayers and retained this behaviour for approximately an hour. Nevetheless, many molecules dissociated, since a large decrease in brightness can be observed. Roughly from this point on immobilised proteins started to appear on the images, although it cannot be excluded that these aggregations were present from the beginning on, but not visible due to the high surface density. However, after almost two hours no mobile fraction was present.

Based on these observations the developed desorption model (Equation 4.3) was fitted to the protein surface densities calculated over time. For values of experiments at room temperature no vertical offset was included in the fit, since no protein clustering was visible, whereas immobile molecules were observed at 37°C and thus, an offset was fitted. The calculated protein surface densities including the fitted function and off-rate of each functionalised bilayer are visible in Figure 4.8a) and Figure 4.8b), respectively for bilayer temperatures of 21°C and 37°C. All fitted values can be found in Appendix C. Exponential fits were normalised to the determined fit value at t_0 for better comparison (Figure 4.9). Like observed in the raw data, surface density values decreased much faster for bilayers at 37°C compared to 21°C, which is also reflected in higher off-rates. The mean of fitted values resulted in $k_{off,\ 21°C} = (3.7 \pm 1.1) \cdot 10^{-3}$ min^{-1} and $k_{off,\ 37°C} = (3.8 \pm 1.4) \cdot 10^{-2}$ min^{-1} (mean ± sd).

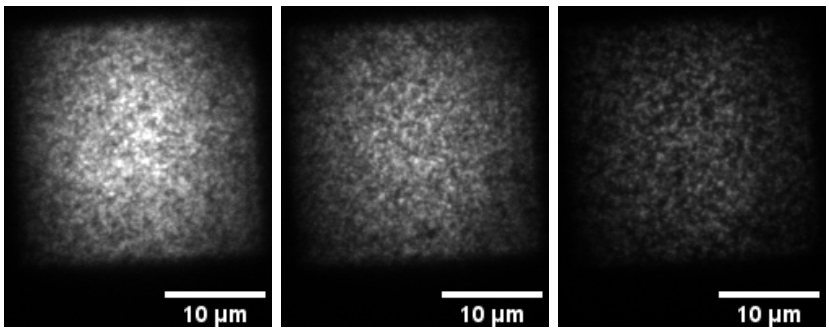

(a) (b) (c)

Figure 4.6.: Bulk brightness of the fluorescently labelled protein IE^K at approximately 21°C over the course of several hours. The first image frame of an acquisition at a) $t = 12$ min, b) $t = 141$ min, c) $t = 273$ min after the washing process of the bilayers was finished is shown. All images have equal brightness scales.

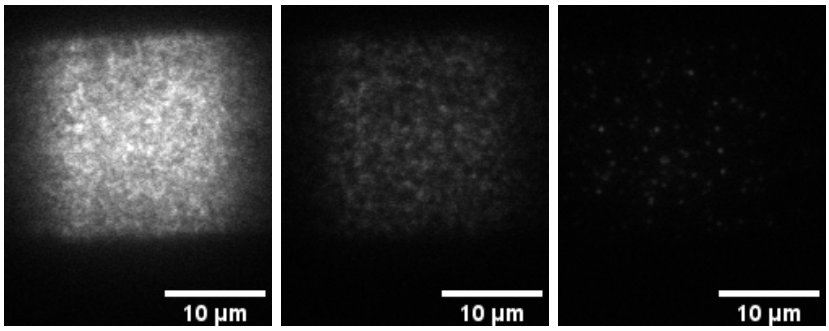

(a) (b) (c)

Figure 4.7.: Bulk brightness of the fluorescently labelled protein IE^K at approximately 37°C over the course of two hours. The first image frame of an acquisition at a) $t = 15$ min, b) $t = 64$ min, c) $t = 115$ min after the washing process of the bilayers was finished is shown. All images have equal brightness scales.

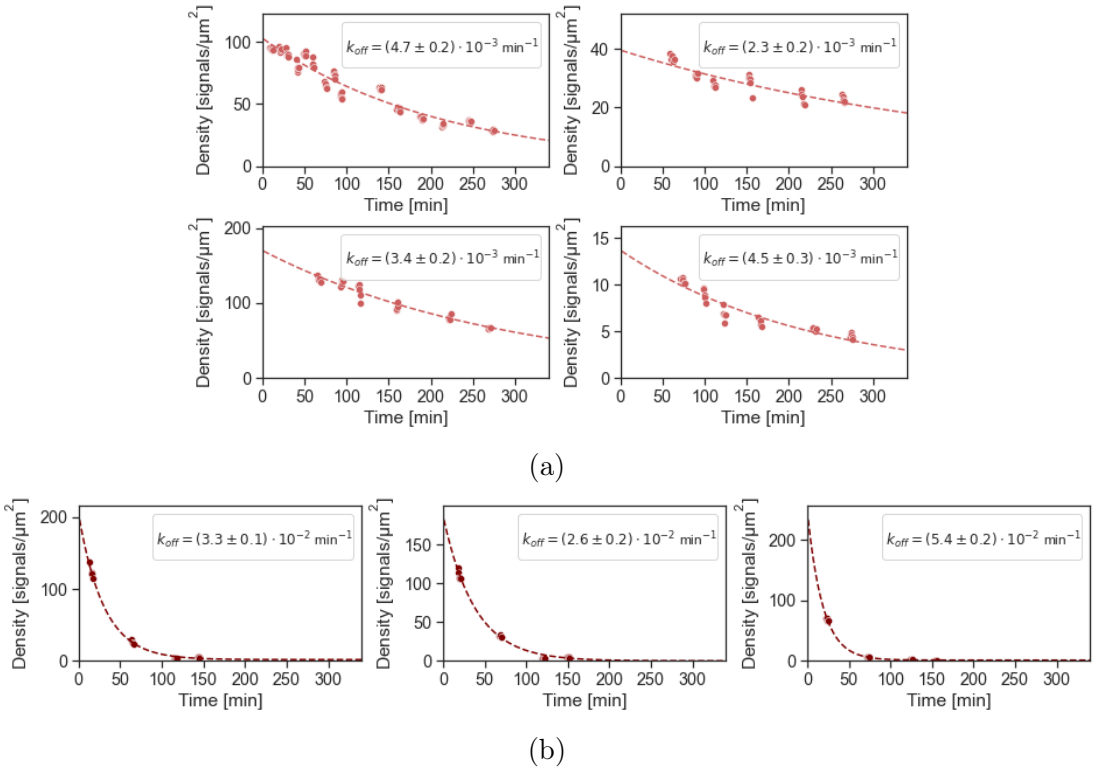

Figure 4.8.: Decrease in density of the fluorescently labelled protein IE^K in experiments at a) 21°C and b) 37°C. Each plot shows the resulting protein surface densities of one bilayer including exponential fit and fitted off-rate.

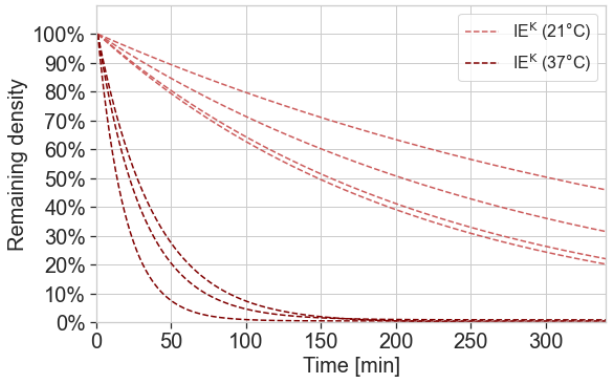

Figure 4.9.: Normalised exponential fits of the decrease in density of the fluorescently labelled protein IE^K. Off-rates (mean ± sd) were $k_{off,\ 21°C} = (3.7 \pm 1.1) \cdot 10^{-3}$ min^{-1} and $k_{off,\ 37°C} = (3.8 \pm 1.4) \cdot 10^{-2}$ min^{-1} respectively for bilayers imaged at 21°C and 37°C.

4.2.2. Trivalent Streptavidin

In general, Streptavidin is a homotetramer that can bind up to four residues. However, triSAV only binds three cystein molecules, each labelled with AF647. The other subunit has a His-tag with six amino acids, that enables the binding to the bilayer (Figure 3.2c). The behaviour of bilayers functionalised with triSAV was observed over almost five hours. Figure 4.10 shows TIRF images of the same bilayer over the course of the experiment. Compared to all other proteins, triSAV showed a lot more aggregations from the beginning of the experiment. Over time, the density of proteins on the bilayer decreased and immobile molecules were more evident. After adding imidazole, only a few fluorescent signals could be detected, of which the majority remained immobile, although a few moving signals were still present. In a subsequent measurement (data not included) it was tested whether the increased fraction of immobile signals in the beginning was bound through the His-tag. For this, a triSAV-funtionalised bilayer was prepared, imaged, imidazole was added and imaged again directly without waiting time. After adding the competing electron donor, hardly any fluorescent signals were present on the images; the ones still visible rarely showed any movement. To quantify this observation, the remaining percentage of bulk brightness within the ROI was determined and resulted in around 3%. Since immobilised proteins detached from the bilayer when imidazole was added, it can be concluded that they are indeed bound through the His-tag and do not stick to the glass plate. Consequently, the higher amount of immobile clusters is not caused by the bilayer quality but more likely by the protein itself. The reason for this behaviour remains a question of interest.

Increasing the bilayer temperature to 37°C generally led to faster protein aggregation. Three images of a bilayer at different timepoints can be seen in Figure 4.11. Like observed in the beginning of the experiment at room temperature, bilayers showed a higher fraction of immobile clusters compared to all other proteins. The visible amount of immobilisations increased constantly, so that after around one hour the majority of detected signals did not move, although a few mobile molecules could still be observed. Nevertheless, after two hours hardly any moving particles were visible.

The developed exponential model (Equation 4.3) was fitted to the calculated protein surface density values; the offset was included for bilayers at both temperature conditions since in both cases a large fraction of immobile clusters was visible in the raw data. Surface densities, exponential fits and determined rate constants are shown in Figure 4.12. The fitted values can be found in Appendix C. Fitted functions were again normalised to the initial fitted value at t_0 (Figure 4.13). In this case, the off-rates did not deviate from each other as much as the determined off-rates for the other proteins. Mean values of the fitted off-rates resulted in $k_{off,\ 21°C} = (1.3 \pm 0.4) \cdot 10^{-2}$ min^{-1} and $k_{off,\ 37°C} = (1.9 \pm 0.5) \cdot 10^{-2}$ min^{-1} (mean

± sd), respectively for bilayer temperatures of 21°C and 37°C. Interestingly, after adding imidazole to bilayers at 21°C, calculated surface densities resulted in values close to zero. For 37°C bilayers the remaining density was higher and approximately equal to the determined offset. This result is another indication, that triSAV immobilisations at 21°C are indeed bound through the His-tag and caused by the protein. On the other hand, at higher temperature they are not bound through the interaction with Ni ions and probably stick to the glass plate.

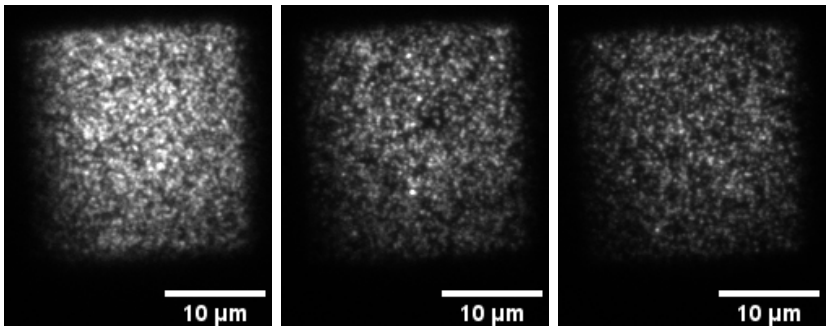

(a) (b) (c)

Figure 4.10.: Bulk brightness of the fluorescently labelled protein triSAV at approximately 21°C over the course of several hours. The first image frame of an acquisition at a) $t = 8$ min, b) $t = 130$ min, c) $t = 285$ min after the washing process of the bilayers was finished is shown. All images have equal brightness scales.

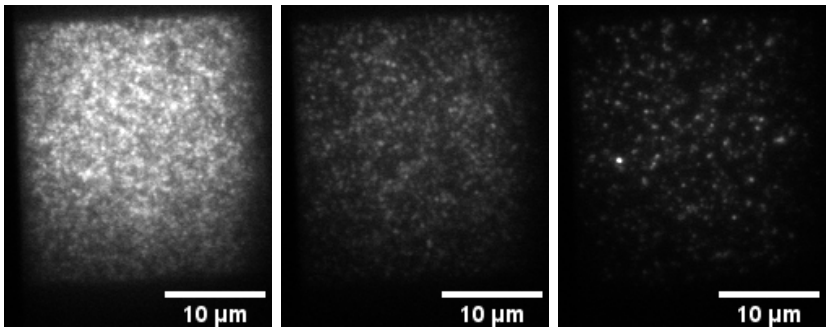

(a) (b) (c)

Figure 4.11.: Bulk brightness of the fluorescently labelled protein triSAV at approximately 37°C over the course of several hours. The first image frame of an acquisition at a) $t = 10$ min, b) $t = 99$ min, c) $t = 200$ min after the washing process of the bilayers was finished is shown. All images have equal brightness scales.

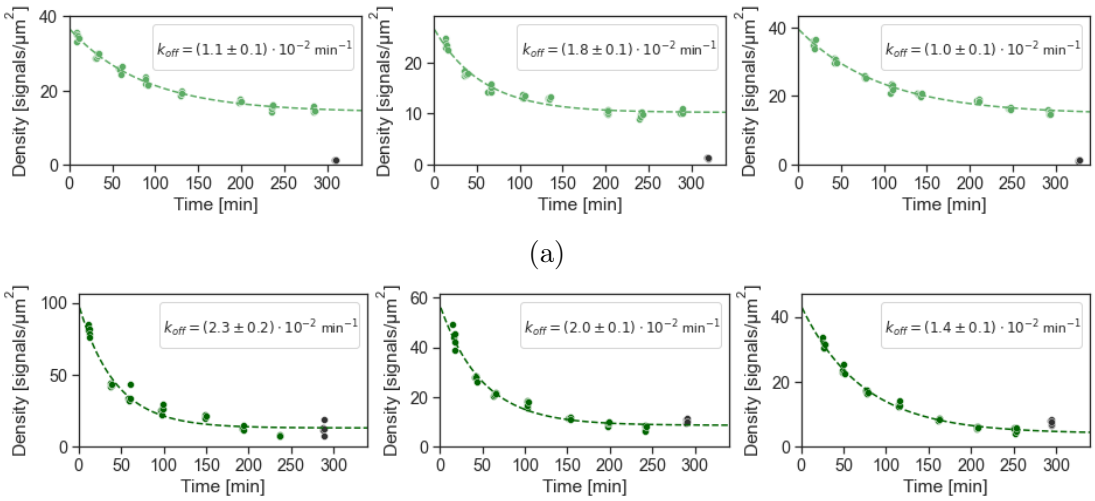

(a)

(b)

Figure 4.12.: Decrease in density of the fluorescently labelled protein triSAV in experiments at a) 21°C and b) 37°C. Each plot shows the resulting protein surface densities of one bilayer including exponential fit and fitted off-rate. Black data points display protein surface densities after adding 50 µl of 1 M in H_2O imidazole buffer solution; these data points were not included in the fits.

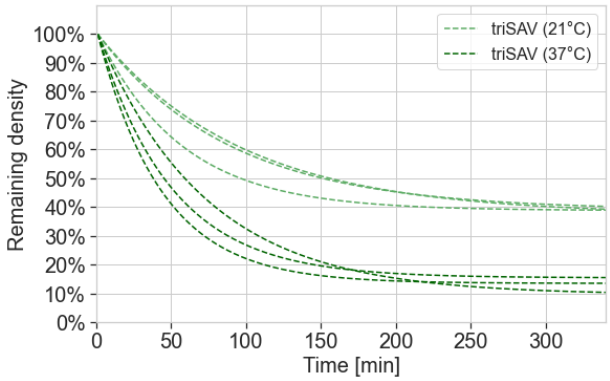

Figure 4.13.: Normalised exponential fits of the decrease in density of the fluorescently labelled protein triSAV. Off-rates (mean ± sd) were $k_{off,\ 21°C} = (1.3 \pm 0.4) \cdot 10^{-2}$ min^{-1} and $k_{off,\ 37°C} = (1.9 \pm 0.5) \cdot 10^{-2}$ min^{-1} respectively for bilayers imaged at 21°C and 37°C.

4.2.3. Divalent Streptavidin

The protein diSAV has two biotin-binding subunits, which are each labelled with a fluorophore. The binding to the Ni-NTA substrate is achieved through two His-tags on the other subunits. Similarly to the previously described proteins, the behaviour of diSAV-functionalised bilayers was observed over nearly five hours at room temperature. An example of a bilayer at three different timepoints is given in Figure 4.14. Proteins showed mobile behaviour during the whole experiment, although a very small immobile fraction was present on each bilayer from the beginning on. A slight reduction in brightness can be observed, but the decrease was not as apparent compared to the other protein with two His-tags (IE^K).

When increasing the temperature to physiological conditions (37°C), the behaviour of diSAV was similar in the beginning of the experiment. Three TIRF images of an exemplary bilayer at different timepoints are visible in Figure 4.15. Again, a few immobile molecules were visible, but the main fraction of proteins showed mobile behaviour. Over time, the brightness decreased considerably and from around 90 minutes, more immobile molecules and bigger protein clusters appeared on the bilayers. After approximately 150 minutes only the immobile fraction was present on the images. To test the specificity of binding, imidazole was added to one bilayer. However, protein aggregates did not dissociate, but rather appeared increased in size. This indicates that remaining clusters are probably not bound through the Ni-His-interaction and in addition, that freely dissolving molecules can reattach to these clusters.

Due to these observations, the offset was not included in the desorption model (Equation 4.3) fitted to surface densities of diSAV at 21°C, but in the model for values at 37°C it was. Calculated densities with exponential fits and determined off-rates for each bilayer are visible in Figure 4.16. The resulting values of the fitted functions can be found in Appendix C. Exponential fits normalised to the value at t_0 can be seen in Figure 4.17. Mean off-rates resulted in $k_{off,\ 21°C} = (1.2 \pm 0.6) \cdot 10^{-3}$ min^{-1} and $k_{off,\ 37°C} = (3.4 \pm 1.5) \cdot 10^{-2}$ min^{-1} (mean ± sd) respectively for bilayers imaged at 21°C and 37°C. Increased off-rates of proteins at physiological conditions reflect the faster dissociation behaviour observed in the raw data. Interestingly, calculated surface densities increased again after around 100 min. Also the values determined after adding imidazole (black data points in Figure 4.16; not included in the fit) were a little bit higher compared to earlier determined values. This result confirms the observation in the raw data and is probably another sign that more proteins accumulate over time and increase the cluster size.

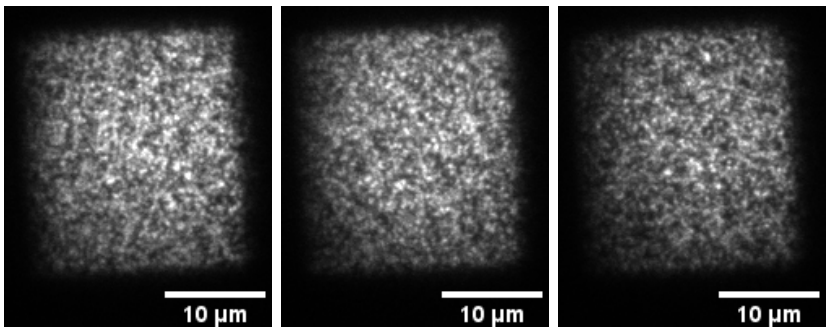

(a) (b) (c)

Figure 4.14.: Bulk brightness of the fluorescently labelled protein diSAV at approximately 21°C over the course of several hours. The first image frame of an acquisition at a) $t = 20$ min, b) $t = 113$ min, c) $t = 245$ min after the washing process of the bilayers was finished is shown. All images have equal brightness scales.

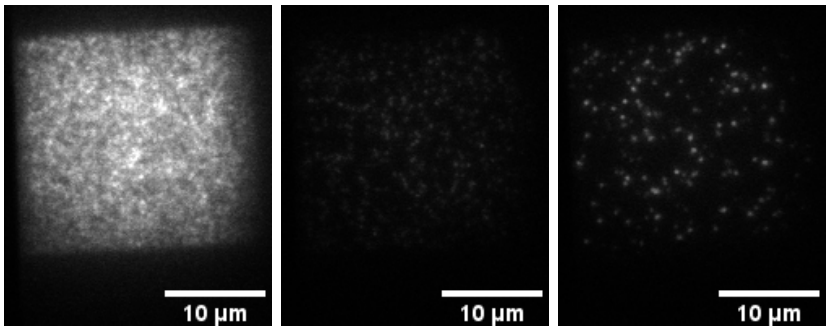

(a) (b) (c)

Figure 4.15.: Bulk brightness of the fluorescently labelled protein diSAV at approximately 37°C over the course of several hours. The first image frame of an acquisition at a) $t = 14$ min, b) $t = 105$ min, c) $t = 155$ min after the washing process of the bilayers was finished is shown. All images have equal brightness scales.

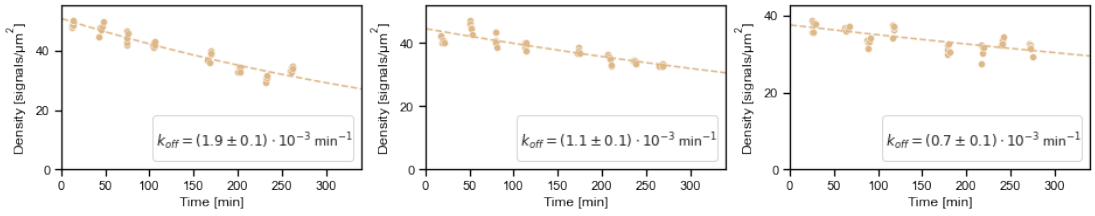

(a)

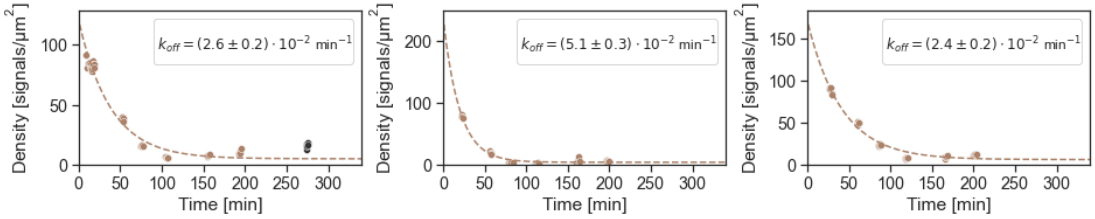

(b)

Figure 4.16.: Decrease in density of the fluorescently labelled protein diSAV in experiments at a) 21°C and b) 37°C. Each plot shows the resulting protein surface densities of one bilayer including exponential fit and fitted off-rate. Black data points display protein surface densities after adding 50 µl of 1 M in H_2O imidazole buffer solution; these data points were not included in the fits.

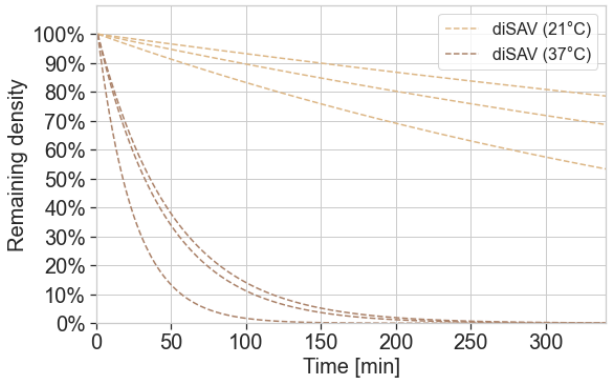

Figure 4.17.: Normalised exponential fits of the decrease in density of the fluorescently labelled protein triSAV. Off-rates (mean ± sd) were $k_{off,\ 21°C} = (1.2 \pm 0.6) \cdot 10^{-3}$ min^{-1} and $k_{off,\ 37°C} = (3.4 \pm 1.5) \cdot 10^{-2}$ min^{-1} respectively for bilayers imaged at 21°C and 37°C.

4.2.4. Monovalent Streptavidin

The third type of Streptavidin used for this thesis was monovalently labelled, i.e. it only had one biotin-binding subunit and three His-tags. The behaviour at room temperature was again assessed over five hours. Three exemplary images of a bilayer during the experiment are depicted in Figure 4.18. No major change in overall brightness and thus protein density is visible. Furthermore, mSAV was mobile on the bilayers during the whole observed period.

Compared to all other proteins, this Streptavidin version retained its mobile behaviour for the longest period when the bilayer temperature was increased to physiological conditions (37°C). Images of a bilayer at three different timepoints during the experiment can be seen in Figure 4.19. During the first hour, no apparent change in brightness could be detected, but after approximately this time, the overall brightness started to decrease. First protein aggregates appeared after almost two hours and hardly any mobile molecules were present on the bilayers after another thirty minutes. Similar to other experiments with bilayer temperatures of 37°C, no change in appearance could be observed when imidazole was added.

Based on these observations the decrease in protein surface density was again modelled (Equation 4.3); the offset was only included in the fit for the higher imaging temperature. Calculated values plotted over time with fitted exponential functions and off-rates can be seen in Figure 4.20 and Figure 4.21 depicts the functions normalised to the fitted value at t_0. The fitted values can be found in Appendix C. Like expected from the behaviour observed in the raw data, this protein showed the smallest off-rates at 21°C, but values for 37°C were in similar orders of magnitude as for the other proteins. The mean of fitted off-rates resulted in $k_{off,\ 21°C} = (5.6 \pm 0.4) \cdot 10^{-4}$ min^{-1} and $k_{off,\ 37°C} = (1.3 \pm 0.2) \cdot 10^{-2}$ min^{-1} (mean ± sd).

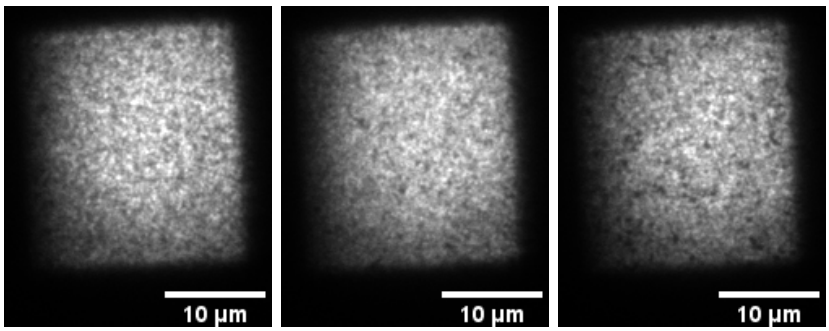

(a) (b) (c)

Figure 4.18.: Bulk brightness of the fluorescently labelled protein mSAV at approximately 21°C over the course of several hours. The first image frame of an acquisition at a) $t = 21$ min, b) $t = 97$ min, c) $t = 260$ min after the washing process of the bilayers was finished is shown. All images have equal brightness scales.

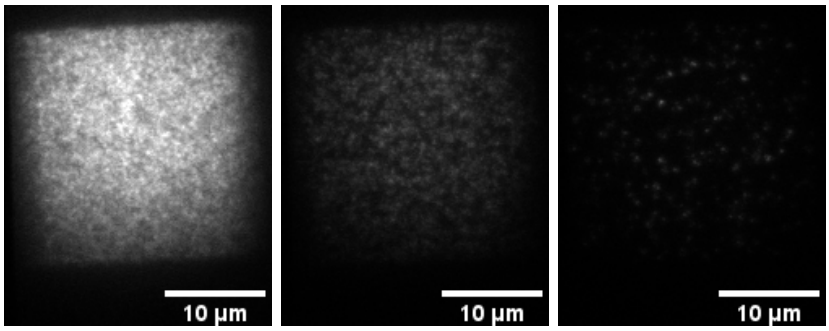

(a) (b) (c)

Figure 4.19.: Bulk brightness of the fluorescently labelled protein mSAV at approximately 37°C over the course of several hours. The first image frame of an acquisition at a) $t = 17$ min, b) $t = 126$ min, c) $t = 201$ min after the washing process of the bilayers was finished is shown. All images have equal brightness scales.

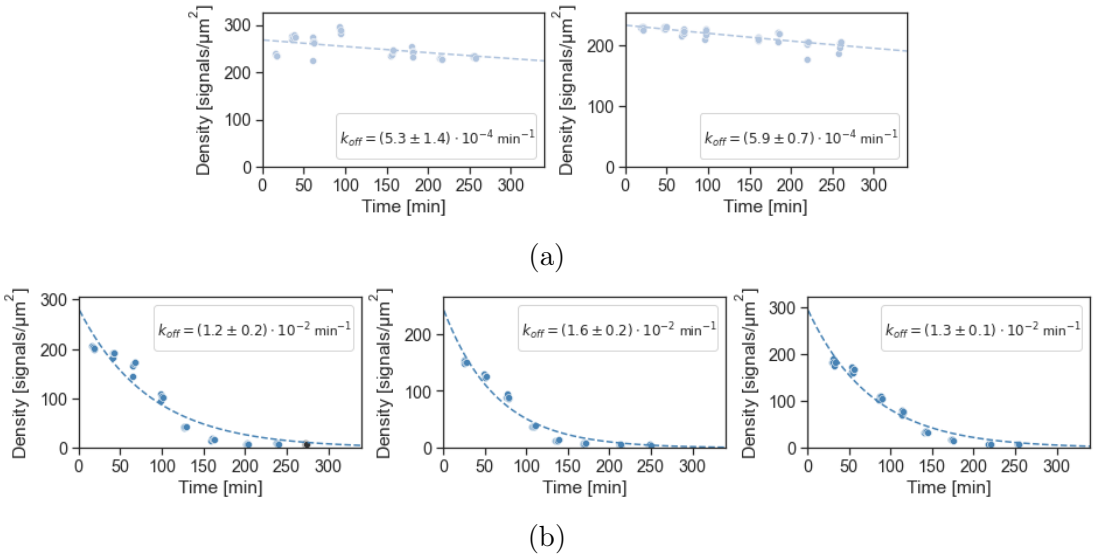

Figure 4.20.: Decrease in density of the fluorescently labelled protein mSAV in experiments at a) 21°C and b) 37°C. Each plot shows the resulting protein surface densities of one bilayer including exponential fit and fitted off-rate. Black data points display protein surface densities after adding 50 µl of 1 M in H_2O imidazole buffer solution; these data points were not included in the fits.

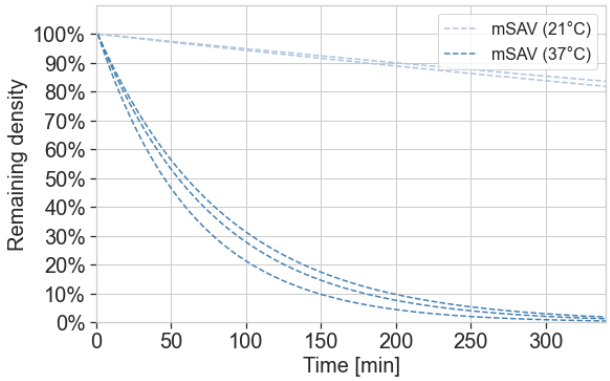

Figure 4.21.: Normalised exponential fits of the decrease in density of the fluorescently labelled protein mSAV. Off-rates (mean ± sd) were $k_{off,\ 21°C} = (5.6 \pm 0.4) \cdot 10^{-4}$ min^{-1} and $k_{off,\ 37°C} = (1.3 \pm 0.2) \cdot 10^{-2}$ min^{-1} respectively for bilayers imaged at 21°C and 37°C.

4.2.5. Comparison

For better comparison normalised fitted exponential functions are shown in Figure 4.22a) and 4.22b), respectively for bilayer temperatures of 21°C and 37°C and the mean values of determined rate constants are summed up in Table 4.1. All resulting values of the fitted model can be found in Appendix C. Like expected, off-rates decreased with increasing number of His-tags when bilayers were incubated at approximately 21°C. triSAV with only one tag showed the highest off-rates. Determined values for proteins with two His-tags, IE^K and diSAV, were in similar orders of magnitude; however, the latter yielded slightly larger rates. Noticeably, the surface density of the protein with the largest number of His-tags, mSAV, remained the most stable and resulted in the smallest off-rates. Fitted models included offsets only in one case, namely for surface densities of triSAV. Compared to all other cases at room temperature conditions, this protein aggregated on bilayers and the offset is intended to reflect the immobilised fraction.

Increasing the bilayer temperature to around 37°C resulted in off-rates within the same order of magnitude for all studied proteins. Interestingly, surface densities of IE^K and diSAV decreased faster than triSAV densities, which is reflected in higher off-rates. Again, slightly slower decrease and thus also smaller rates were determined for mSAV. Fitted models always included an offset, since all proteins immobilised and formed aggregates on bilayers at physiological conditions. However, nearly all determined values were close to or approximately zero. Offsets for surface densities of triSAV resulted in slightly higher values, which can probably be attributed again to a higher fraction of immobilized proteins right from the beginning.

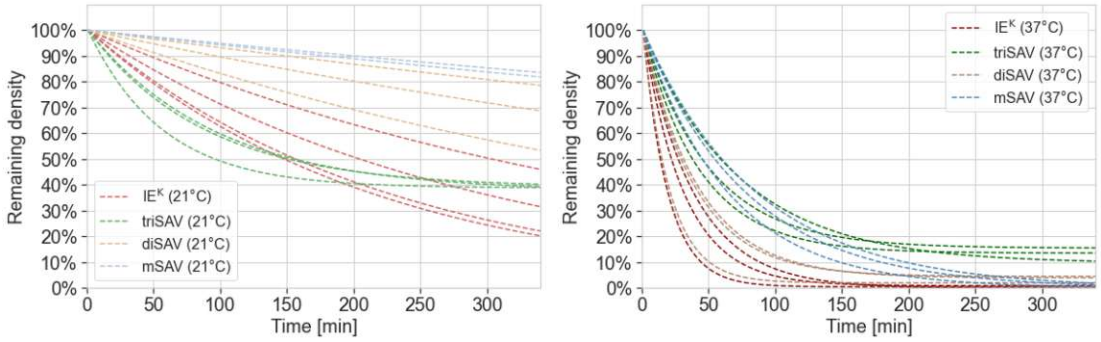

(a) (b)

Figure 4.22.: Comparison of the normalised exponential fits of the decrease in density of the fluorescently labelled proteins IE^K, triSAV, diSAV, mSAV in experiments at a) 21°C and b) 37°C.

Table 4.1.: Summary of calculated means ± sd of all fitted off-rates.

Protein	His-tags	$k_{off,\ 21°C}$ [min^{-1}] (mean ± sd)	$k_{off,\ 37°C}$ [min^{-1}] (mean ± sd)
IE^K	2	$(3.7 \pm 1.1) \cdot 10^{-3}$	$(3.8 \pm 1.4) \cdot 10^{-2}$
triSAV	1	$(1.3 \pm 0.4) \cdot 10^{-2}$	$(1.9 \pm 0.5) \cdot 10^{-2}$
diSAV	2	$(1.2 \pm 0.6) \cdot 10^{-3}$	$(3.4 \pm 1.5) \cdot 10^{-2}$
mSAV	3	$(5.6 \pm 0.4) \cdot 10^{-4}$	$(1.3 \pm 0.2) \cdot 10^{-2}$

4.3. Protein desorption after recharging NTA binding sites

To improve the stability of protein binding, bilayers were incubated with 100 mM $NiCl_2$ for 5 minutes before functionalisation with the protein IE^K. This step was conducted to ensure that free NTA sites were recharged with Ni ions and are also available for the coordination bond. The behaviour of functionalised bilayers in physiological conditions was inspected over more than three hours; exemplary bilayer images at three different timepoints during the experiment can be seen in Figure 4.23. In the beginning molecules were mobile and showed similar behaviour like proteins on bilayers without the recharging step. However, compared to this experiment, the density seems to decrease faster, since only a few signals could be detected after approximately an hour. Nevertheless, they remained mobile up to two hours after conducting the washing process. From this point on, immobile aggregates started to appear and after roughly another hour only bright immobile clusters were visible.

Protein surface densities were again determined over time and the developed exponential model (Equation 4.3) fitted including an offset, since protein clusters appeared on the bilayers. Calculated density values including the fitted functions and off-rates are visible in Figure 4.24. The resulting fitted values can be found in Appendix C. Exponential fits normalised to the initial fit value at t_0 can be seen in Figure 4.25. They are compared to determined normalised functions for decreasing IE^K surface densities on bilayers without recharging ($k_{off,\ 37°C} = (3.8 \pm 1.4) \cdot 10^{-2}$ min^{-1}), where the data was shown in subsection 4.2.1. Off-rates were generally a little bit higher, but still resulted in similar orders of magnitude, with a mean of $k_{off,\ 37°C,\ \text{NTA-recharging}} = (5.4 \pm 1.8) \cdot 10^{-2}$ min^{-1} (mean ± sd). Increased values indicate faster decrease in surface density, which was also observed in the raw data.

Consequently, recharging of available NTA sites did not yield considerable improvement regarding protein desorption from bilayers in physiological conditions in this experiment, although it led to a delay of immobilisations.

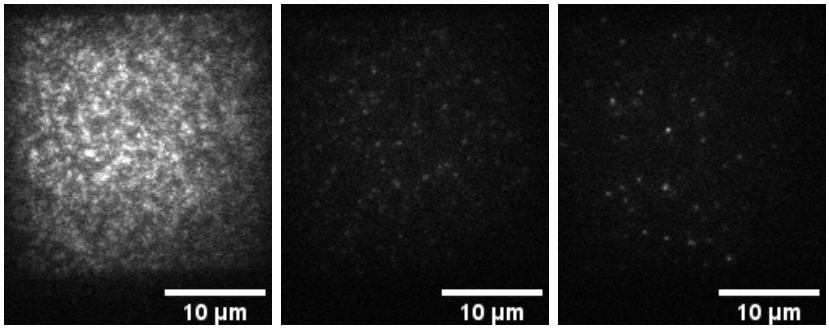

(a) (b) (c)

Figure 4.23.: Bulk brightness of the fluorescently labelled protein IE^K at approximately 37°C over the course of several hours after bilayers were recharged with $NiCl_2$. The first image frame of an acquisition at a) $t = 16$ min, b) $t = 60$ min, c) $t = 174$ min after the washing process of the bilayers was finished is shown. All images have equal brightness scales.

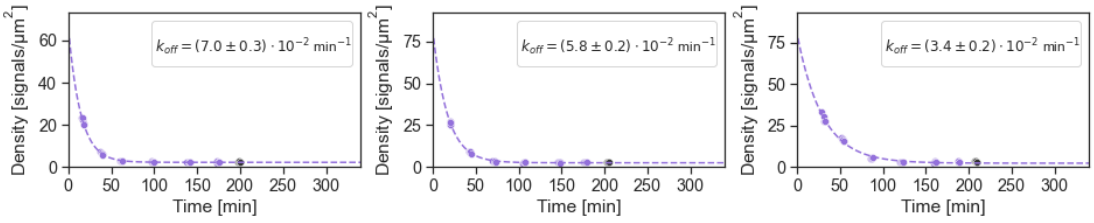

(a)

Figure 4.24.: Decrease in density of the fluorescently labelled protein IE^K in experiments at 37°C after recharging of potential free Ni-binding sites of the NTA adsorbent. Each plot shows the resulting protein surface densities of one bilayer including exponential fit and fitted off-rate. Black data points display protein surface densities after adding 50 µl of 1 M in H_2O imidazole buffer solution; these data points were not included in the fits.

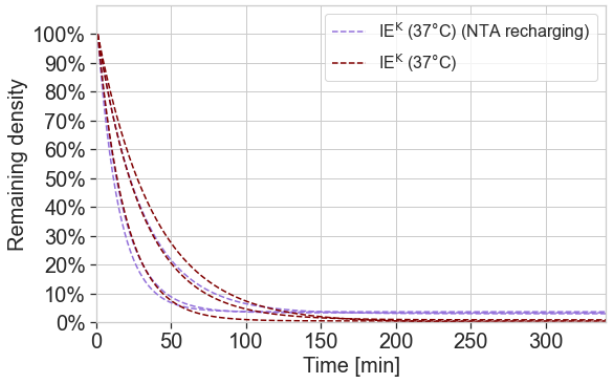

Figure 4.25.: Normalised exponential fits of the decrease in density of the fluorescently labelled protein IE^K at 37°C with and without recharging of potential free Ni-binding sites. Off-rates (mean ± sd) were $k_{off,\ 37°C,\ \text{NTA-recharging}} = (5.4 \pm 1.8) \cdot 10^{-2}$ min^{-1} and $k_{off,\ 37°C} = (3.8 \pm 1.4) \cdot 10^{-2}$ min^{-1} respectively for bilayers imaged at 21°C and 37°C.

4.4. Protein desorption in dependence on HBSS buffer pH

In protein purification systems the elution of proteins is achieved by lowering the pH of the buffer. Consequently, increasing the pH could possibly improve the binding stability. To test whether the pH of the buffer influences the binding, IE^K-functionalised bilayers were studied with three different HBSS buffer conditions at physiological temperatures. For one bilayer, the buffer was not altered. For the other two bilayers, HBSS buffers with pH = 8 and pH = 8.5 were prepared by adding 1 M NaOH to the solution prior to washing. The pH was measured at room temperature (21°C) before the buffers were exchanged.

The behaviour of functionalised bilayers with HBSS buffer at pH = 8 and pH = 8.5 at three different timepoints during the experiment can be seen in Figure 4.26 and Figure 4.27 respectively. Images of bilayers with unchanged pH from this experiment were not included, since they behaved similar compared to bilayers shown in Figure 4.7. Fast decrease in density could be observed and after approximately 2.5 hours only immobilised molecules were present on bilayers.

When the pH of the buffer was increased to 8 the behaviour of proteins did not change much compared to previously observed bilayers. Although slight improvement was visible, as some mobile molecules were still present after 2 hours, they dissociated within the next 30 minutes and only the immobilised fraction remained

after 2.5 hours.

However, increasing the pH of the buffer to 8.5 yielded considerable improvement. The overall brightness of bilayers did not decrease as much as previously observed and the main fraction of proteins stayed mobile during the observed period of 3.5 hours. Nevertheless, some immobile aggregates appeared over the course of the experiment.

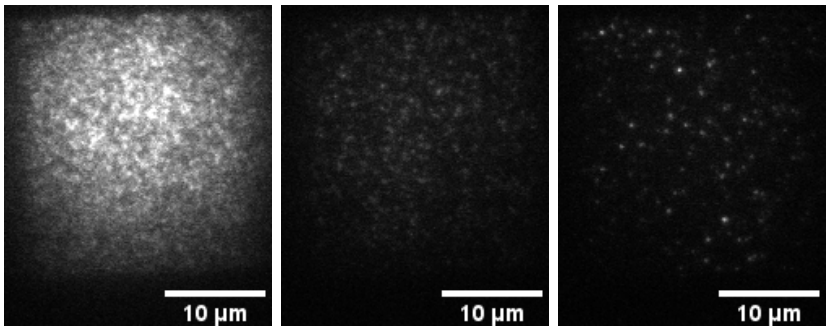

(a) (b) (c)

Figure 4.26.: Bulk brightness of the fluorescently labelled protein IE^K at approximately 37°C over the course of two hours with HBSS pH = 8. The first image frame of an acquisition at a) $t = 26$ min, b) $t = 75$ min, c) $t = 152$ min after the washing process of the bilayers was finished is shown. All images have equal brightness scales.

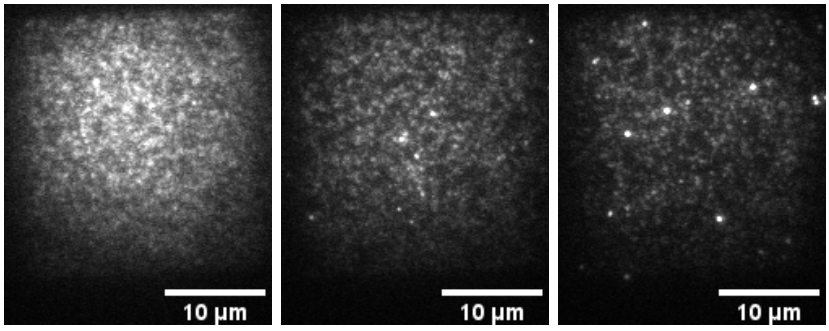

(a) (b) (c)

Figure 4.27.: Bulk brightness of the fluorescently labelled protein IE^K at approximately 37°C over the course of several hours with HBSS pH = 8.5. The first image frame of an acquisition at a) $t = 30$ min, b) $t = 113$ min, c) $t = 219$ min after the washing process of the bilayers was finished is shown. All images have equal brightness scales.

The developed desorption model (Equation 4.3) was again fitted to the calculated protein surface densities of IE^K for each bilayer (Figure 4.28). Resulting values of the fit be found in Appendix C. The offset was included for every buffer pH condition. In the case of pH = 8.5 the model was furthermore fitted without an offset for comparison, since this was the only case where proteins remained mobile. The off-rate of the bilayer with unchanged HBSS buffer resulted in $k_{off,\ \mathrm{pH7.5}} = (2.3 \pm 0.2) \cdot 10^{-2}\ \mathrm{min}^{-1}$ (mean ± sd), which is in similar range to other determined off-rates for IE^K at 37°C (compare Figure 4.8b). For buffer pH = 8 the off-rate $k_{off,\ \mathrm{pH8}} = (6.5 \pm 0.2) \cdot 10^{-2}\ \mathrm{min}^{-1}$ (mean ± sd) was slightly increased, but still within the same order of magnitude. The model including the offset for the bilayer with buffer pH = 8.5 also determined an off-rate in similar range with $k_{off,\ \mathrm{pH8.5}} = (1.4 \pm 0.2) \cdot 10^{-2}\ \mathrm{min}^{-1}$ (mean ± sd). However, without offset the fitted rate was much smaller and resulted in $k_{off,\ \mathrm{pH8.5}} = (5.8 \pm 0.2) \cdot 10^{-3}\ \mathrm{min}^{-1}$ (mean ± sd).

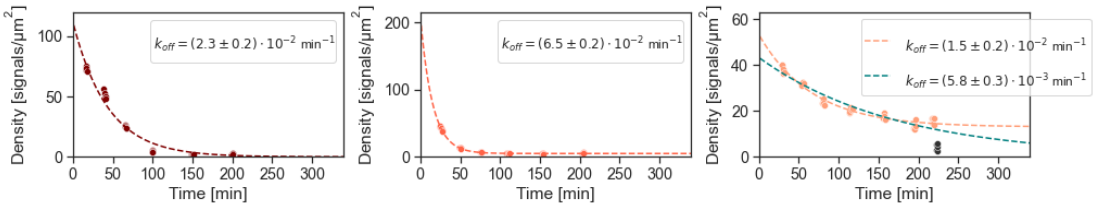

(a)

Figure 4.28.: Decrease in density of the fluorescently labelled protein IE^K in experiments at 37°C with different HBSS buffer pH conditions: pH = 7.5 (left), pH = 8 (middle), pH = 8.5 (right). Each plot shows the resulting protein surface densities of one bilayer including exponential fit and fitted off-rate. For the bilayer with HBSS pH = 8.5 the model was fitted with offset (orange curve) and without offset (blue curve). Black data points display protein surface densities after adding 50 µl of 1 M in H_2O imidazole buffer solution; these data points were not included in the fits.

5. Discussion

In this thesis, temperature dependent effects on the stability of protein functionalised SLBs have been examined. This is important, since SLBs are used to study the activation behaviour of T cells under physiological temperature conditions. To model the activation and prevent experimental artefacts, stable bilayers and protein behaviour are required. The intention of this thesis was to determine how bilayers functionalised with various proteins behave at two temperature conditions, so that potential influences for T cell experiments can be identified.

5.1. Bilayer stability and lipid detachment

In ideal conditions it would be expected that no change occurs in the bilayer, since the lipids should remain on the glass slip. However, in reality it may be possible that lipids detach and holes form in the bilayer. As a consequence, proteins may be able to accumulate and influence the analysis, since they are no longer bound through the Ni-His-interaction, but are still present. To characterise how the bilayer behaves, a tracer lipid (DOPE-Atto488) was included in the vesicle composition.

In general, the bilayers were still present and lipids remained mobile until the end of the observed periods for both temperature conditions. The overall brightness of bilayers in room temperature conditions did not change (Figure 4.1), but physiological temperatures led to slight decrease and holes appeared over the course of the experiment (Figure 4.2). Even though, no evident holes were visible in the raw data of room temperature bilayers, it cannot be excluded that some were present, as they could lie below the diffraction limit and are therefore too small to be visible. Besides, in preliminary experiments (data not included) minor holes were also observed under the same conditions.

In order to quantify this observation, the background corrected intensity was determined over time. It has to be mentioned, that brightness values cannot be compared between experiments on different days due to variations in the laser intensity. For better comparison an exponential function (without offset) was fitted and off-rates were determined (Figure 4.3). The results confirmed the behaviour observed in the raw data. Off-rates of bilayers at 21°C were rather smaller (mean ± sd of three bilayers: $k_{off,\ 21°C} = (2.8 \pm 3.9) \cdot 10^{-5}\ \mathrm{min}^{-1}$), which indicates almost no

decrease. One off-rate even resulted in the range of 10^{-24} min^{-1} (Figure 4.3a, left); this value arises probably due to statistical intensity fluctuations of the imaged bilayer surface. When the temperature of bilayers was increased to physiological conditions, off-rates were 100-times greater (mean ± sd of nine bilayers: $k_{off,\ 37°C} = (1.1 \pm 0.3) \cdot 10^{-3}$ min^{-1}), which reflects the observed decrease in overall intensity.

Why more lipids detach from the glass plate at higher bilayer temperature is not quite clear. Also other factors like photobleaching or the general quality of bilayers on a particular day may play a role. The latter could be influenced by lipid degradation, due to insufficient protection against oxygen, or by irregular cleaning of the glass plate caused by the plasma chamber. Nevertheless, care was taken to ensure precise and accurate work, so that experimental conditions were equal on each day.

Seeing these results, it cannot be denied that bilayers remain more stable at 21°C, but the effect of lipid detachment is rather slow and presumably not the primary reason for the decrease in protein density.

5.2. Modelling protein desorption

Since brightness values cannot be compared between experiments on different days, protein surface densities were calculated with the background corrected intensity and the SMB. Here it needs to be mentioned, that the emission characteristics of AF647 are temperature dependent and the fluorescent intensity decreases to roughly 60% for 37°C compared to 21°C [56]. Consequently, the temperature of bilayers with high protein density and bilayers with low protein density should be equal, so that both the bulk brightness and the SMB decrease proportionally. However, this effect would only cause an error, if the SMB would not be determined at the same time or temperature.

There are several factors which could influence the protein surface density. Bulk brightness values could be overestimated due to a higher contribution of the fluorescent background when the protein density is rather low towards the end of experiments. Furthermore, in two colour measurements the red and the blue laser were operated simultaneously for high density bilayers, but not for low density bilayers. Due to the simultaneous operation, there is a small probably that AF647 fluorophores also get excited by the blue laser and thus cause an increase in bulk brightness. However, this is a systematic error and affects all calculated values, but does not change the overall trend in the data. Likewise, the SMB is prone to errors and influenced by photobleaching. In particular, brightness values of triSAV and diSAV, which are labelled with more than one fluorophore may be underestimated, as single fluorophores could be bleached and therefore reduce mean values per protein. Besides that, non-monomeric structures like clusters or coincidental

encounters of fluorophores on images may lead to falsified values. To counteract such artefacts, the localisation data was filtered. Due to these reasons, absolute protein surface densities may be falsified. However, they still give a valid impression about the desorption behaviour of proteins, since the change over time was of interest.

The decrease in density was modelled with a mono-exponential function (Equation 4.3). Here, the question arises, whether a one-step unbinding model accurately represents the molecular desorption process. In the literature a two-step unbinding process is proposed [18]. However, since it is not possible to get insight on the exact unbinding mechanism with the used imaging modality and to determine whether proteins bind poylvalently or if there is a change from poly- to monovalent binding, a mono-exponential approach is more feasible.

Concerning the statistical power of the conducted experiments, it needs to be said, that two, three or four bilayers is statistically speaking not a particular large number. Thus, the statistical power of calculated mean rates is limited. Concerning the fitted value of the initial protein surface density (RL_0), no data is available at this timepoint and consequently this value will not reflect the true density in the beginning. Even though a compromise had to be made between the number of observed bilayers and the number of datapoints acquired for each bilayer, a clear trend is visible in the data and the differences between the observed proteins are undeniably evident.

5.2.1. Protein desorption at ambient temperature conditions

All proteins stayed mobile on bilayers during the experiments, although a decrease in surface density occurred for each probe. Only in the case of triSAV noticeable aggregates were present and the density seemed to stay almost constant after two hours. Due to this, it was the only case where an offset was included in the model. Like expected, off-rates for this protein resulted in the highest values (mean ± sd of three bilayers: $k_{off,\ 21°C} = (1.3 \pm 0.4) \cdot 10^{-2}\ \text{min}^{-1}$). Nevertheless, the observed decrease of triSAV is similar to the unbinding of GFP, also with a single His-tag, reported by Nye et al. [18]. After 5 hours approximately 40% of GFP remained on the bilayer, which is identical with the percentage of triSAV densities determined by the fitted model after 5 hours.

Not surprisingly, fitted off-rates decreased for surface densities of proteins with two His-tags. They were approximately by a factor of 10 smaller compared to triSAV (mean ± sd of three diSAV-functionalised bilayers: $k_{off,\ 21°C} = (1.2 \pm 0.6) \cdot 10^{-3}\ \text{min}^{-1}$, mean ± sd of four IE^K-functionalised bilayers: $k_{off,\ 21°C} = (3.7 \pm 1.1) \cdot 10^{-3}\ \text{min}^{-1}$). Interestingly, all off-rates of diSAV were smaller than off-rates of IE^K at room temperature. The reason for this observation is not quite clear and could be caused by several influences. For instance, it could be possible that

Ni-binding sites are better accessible by diSAV compared to IE^K due to sterical reasons.

Off-rates even decreased further for mSAV with three His-tags and resulted in values approximately 10 times smaller (mean ± sd of two bilayers: $k_{off,\ 21°C} = (5.6 \pm 0.4) \cdot 10^{-4}\ \text{min}^{-1}$). This observation is consistent with literature [20], since it was expected that the binding is more stable when the number of His-tags increases.

5.2.2. Protein desorption at physiological temperature conditions

An increase in temperature drastically changed the stability of binding and proteins dissociated much faster. After around $2 - 2.5$ hours only immobile molecules were present on bilayers. These aggregations probably stick to the glass plate, since adding imidazole did not yield a change in appearance or calculated values. The off-rate increased for each protein and resulted in the range of $10^{-2}\ \text{min}^{-1}$ (compare Table 4.1). However, mobile proteins were generally retained longer with increasing number of His-tags. This is also visible in calculated densities for mSAV, where the fitted exponential function is not an optimal representation of the decrease in density and thus determined off-rates are probably not as reliable as other fitted values.

However, there are several possible explanations why proteins detach much faster from bilayers at physiological conditions. Partial loss in density could be caused due to lipid detachment and holes in the bilayer, although the influence of this is probably rather small. Another possible explanation could be that Ni ions dissociate from the NTA adsorbent over time and thus proteins can no longer bind. For IE^K it may also be possible that the peptide, which is labelled with the fluorophore, dissociates and thus proteins are still bound but no longer visible. Besides that, also the buffer conditions, like the pH or ion composition could influence the Ni-His-interaction. Furthermore, it needs to be considered that proteins may not be stable at these temperature conditions and denaturation or changes in the conformation occur that lead to the breaking of the bond.

5.3. Protein desorption after recharging NTA binding sites

Recharging of NTA with $NiCl_2$ prior to protein functionalisation was tried to improve the binding stability, since it is possible that Ni ions dissociate from the NTA adsorbent. Apart from a minor improvement in the fraction of proteins that

remained mobile on the bilayers for longer time, the density of IE^K decreased faster compared to bilayers in the experiment without the recharging step. This observation is also reflected in slightly increased off-rates (mean ± sd of three bilayers: $k_{off,\ 37°C,\ \text{NTA-recharging}} = (5.4 \pm 1.8) \cdot 10^{-2}\ \text{min}^{-1}$). Consequently, recharging of binding sites did not yield considerable improvement.

5.4. Protein desorption in dependence on HBSS buffer pH

As second approach to improve the binding stability, the pH of the HBSS buffer was altered. In protein purification systems a possible elution strategy is to lower the pH of the buffer. Lower pH leads to the protonation of the amino acids and reverses the coordination bond. Consequently, by doing the exact opposite, i.e. increasing the pH and deprotonating the His-tag, proteins may be bound more stably over time.

Therefore, HBSS buffers with pH = 8 and pH = 8.5 were prepared and compared to washed bilayers with unchanged HBSS at 37°C. These two values were chosen since they are still within physiological conditions for proteins. Bilayers with buffer pH = 8, did not really show any improvement and the rate constant (mean ± sd: $k_{off,\ \text{pH8}} = (6.5 \pm 0.2) \cdot 10^{-2}\ \text{min}^{-1}$) was in similar order of magnitude as rates of bilayers with unchanged pH.

On the contrary, the stability of binding increased drastically when the pH of the buffer was modified to 8.5. After 3.5 hours a huge fraction of proteins was still mobile, although some aggregates were also present. Surface densities were analogously fitted including a vertical offset. With this model the off-rate did not indicate any improvement (mean ± sd: $k_{off,\ \text{pH8.5}} = (1.5 \pm 0.2) \cdot 10^{-2}\ \text{min}^{-1}$) and also a rather unrealistic value was determined for the offset ($\text{RL}_{\text{const}} = 13 \pm 0.9$ signals/μm^2). As it would be expected that density values still decrease after the observed period, these values probably do not reflect the behaviour accurately. Therefore, the model was fitted without offset. With this approach the determined off-rate was much smaller (mean ± sd: $k_{off,\ \text{pH8.5}} = (5.8 \pm 0.3) \cdot 10^{-3}\ \text{min}^{-1}$) and thereby reflects the observation in the raw data. Smaller off-rates indicate slower desorption and consequently higher binding stability. Due to these results it can be concluded, that the HBSS buffer conditions are not optimal and interfere with the Ni-His coordination bond. For that reason, proteins cannot be retained on bilayers at higher bilayer temperatures over longer periods. Besides, other groups [18–22] used different buffers in their experiments which may be more favourable for the binding. Consequently, the buffer conditions must be chosen carefully.

6. Conclusion & Outlook

The behaviour of SLBs was analysed with the tracer lipid DOPE-Atto488. At ambient temperature no change was visible in the bilayer, but small holes appeared when the temperature was increased to physiological conditions. These findings were also reflected in the background corrected intensity, which showed almost no change for 21°C, but small decrease over time for 37°C.

SLBs functionalised with four different proteins (IE^K, triSAV, diSAV, mSAV) were examined at ambient and physiological temperature conditions. The behaviour of the protein IE^K was of particular interest since it is used as pMHC for T cell studies on SLBs. At ambient temperature conditions all proteins stayed mobile on bilayers, except for triSAV which formed aggregations from the beginning. For IE^K and triSAV even a decrease in density was visible in the raw data. In contrast to this, the surface density of each protein decreased rapidly on bilayers in physiological conditions and after $2 - 2.5$ hours only immobile molecules were present in the images.

A one-step desorption model based on simple receptor-ligand kinetics was developed and fitted to calculated protein surface densities. Not surprisingly, triSAV, with one His-tag had the highest off-rates ($k_{off,\ 21°C} \approx 1.3 \cdot 10^{-2}$ min^{-1}). Off-rates decreased for IE^K ($k_{off,\ 21°C} \approx 3.7 \cdot 10^{-3}$ min^{-1}) and diSAV ($k_{off,\ 21°C} \approx 1.2 \cdot 10^{-3}$ min^{-1}), which both have two His-tags. As expected, mSAV with three His-tags, showed the most stable binding over time ($k_{off,\ 21°C} \approx 5.6 \cdot 10^{-4}$ min^{-1}). When the bilayer temperature was increased to 37°C all off-rates resulted in ranges of approximately 10^{-2} min^{-1}. Seeing this, it can be concluded that elevated temperatures alter the experimental conditions in a way, that they become unfavourable for the Ni-His interaction and proteins dissociate from the bilayer much faster.

Two approaches were tested to improve the binding stability of IE^K at physiological temperatures. In one experiment bilayers were incubated with $NiCl_2$ to recharge potential free NTA binding sites before protein functionalisation. However, no improvement could be achieved. The second approach included varying the pH of the HBSS buffer. At pH = 8 no considerable improvement was visible, but an increase to pH = 8.5 led to much slower desorption and around 50% of proteins were still retained after 3.5 hours. Nevertheless, since these results were not reproduced, artefacts related to the general bilayer quality cannot be excluded.

All in all, every protein showed fast decrease in surface density at physiological conditions. Therefore it can be concluded, that higher off-rates of IE^K are not caused by the protein itself, but that experimental conditions are probably not ideal. The buffer has a huge influence on the binding between His-tags and Ni ions. Due to this, more emphasis should be given on the buffer conditions in future experiments. For instance, ions in the buffer could compete with the Ni ions of the substrate and thereby interfere with the coordination bond. Obviously, analysing the dependence on the pH and determining an optimal range could achieve decreased desorption rates. Besides that, another possible strategy to improve the binding stability involves increasing the number Ni ions, either by using a larger molar fraction of DGS-NTA(Ni) or by using multidenate chelators like trisNTA [43]. Finding ways to improve the binding stability will give valuable information about the interaction of His tagged proteins with Ni-chelated lipids and will hopefully improve experimental conditions both at ambient and physiological temperatures.

Bibliography

[1] Friedrich Marks, Ursula Klingmüller and Karin Müller-Decker. *Cellular Signal Processing*. Second Edition. New York: Garland Science, Taylor & Francis Group, LLC, 2017.

[2] Bruce Alberts et al. *Molecular Biology of the Cell*. Sixth Edition. New York: Garland Science, 2015.

[3] Abul K. Abbas, Andrew H. Lichtman and Shiv Pillai. *Cellular and Molecular Immunology*. ninth. Philadelphia: Elsevier, 2018.

[4] David D. Chapling. 'Overview of the Immune Response'. In: *The Journal of allergy and clinical immunology* 125.2 Suppl 2 (2010), pp. 3–23. DOI: 10.1016/j.jaci.2009.12.980.

[5] Sharon S. Evans, Elizabeth A. Repasky and Daniel T. Fisher. 'Fever and the thermal regulation of immunity: the immune system feels the heat'. In: *Nature Reviews Immunology* 15 (2015), pp. 335–349. DOI: 10.1038/nri3843.

[6] Thomas A Mace et al. 'Differentiation of CD8+ T cells into effector cells is enhanced by physiological range hyperthermia'. In: *Journal of leukocyte biology* 90.5 (2011), pp. 951–962. DOI: 10.1189/jlb.0511229.

[7] Thomas A Mace et al. 'Effector CD8+ T cell IFN-γ production and cytotoxicity are enhanced by mild hyperthermia'. In: *Journal of Hyperthermia* 28.1 (2012), pp. 9–18. DOI: 10.3109/02656736.2011.616182.

[8] E. R. Zynda et al. 'A role for the thermal environment in defining costimulation requirements for CD4(+) T cell activation.' In: *Cell cycle* 14.14 (2015), pp. 2340–2354. DOI: 10.1080/15384101.2015.1049782.

[9] Changdong Lin et al. 'Fever Promotes T Lymphocyte Trafficking via a Thermal Sensory Pathway Involving Heat Shock Protein 90 and α4 Integrins'. In: *Immunity* 50.1 (2019), pp. 137–151. DOI: 10.1016/j.immuni.2018.11.013.

[10] Lukas K. Tamm and Harden M. McConnel. 'Supported Phospholipid Bilayers'. In: *Biophysical Journal* 47.1 (1985), pp. 105–113. DOI: 10.1016/S0006-3495(85)83882-0.

[11] Formation of Solid-Supported Lipid Bilayers: An Integrated View. 'Richter, Ralf P. and Bérat, Rémi and Brisson, Alain R.' In: 22.8 (2006), pp. 3497–3505. DOI: 10.1021/la052687c.

[12] Joshua A. Jackman and Nam-Joon Cho. 'Supported Lipid Bilayer Formation: Beyond Vesicle Fusion'. In: *Langmuir* 36.6 (2020), pp. 1387–1400. DOI: 10.1021/acs.langmuir.9b03706.

[13] Ilja Czolkos, Aldo Jersorka and Owe Orwar. 'Molecular phospholipid films on solid supports'. In: *Soft Matter* 7.10 (2011), pp. 4562–4576. DOI: 10.1039/C0SM01212B.

[14] Eugene Sulkowski. 'Purification of Proteins by IMAC'. In: *Trends in Biotechnology* 3.1 (1985), pp. 1–7. DOI: 10.1016/0167-7799(85)90068-X.

[15] Erich Hochuli, Heinz Döbli and Alfred Schacher. 'New metal chelate adsorbent selective for proteins and peptides containing neighbouring histidine residues'. In: *Journal of Chromatography* 411 (1987), pp. 177–184. DOI: 10.1016/s0021-9673(00)93969-4.

[16] Erich Hochuli et al. 'Genetic Approach to Facilitate Purification of Recombinant Proteins with a Novel Metal Chelate Adsorbent'. In: *Nature Biotechnology* 6 (1988), pp. 1321–1325. DOI: 10.1038/nbt1188-1321.

[17] Joanne Crowe et al. '6xHis-Ni-NTA chromatography as a superior technique in recombinant protein expression/purification'. In: *Methods in Molecular Biology* 31 (1994), pp. 371–387. DOI: 10.1385/0-89603-258-2:371.

[18] Jeffrey A. Nye and Jay T. Groves. 'Kinetic Control of Histidine-Tagged Protein Surface Density on Supported Lipid Bilayers'. In: *Langmuir* 24.8 (2008), pp. 4145–4149. DOI: 10.1021/la703788h.

[19] Steven Knecht et al. 'Oligohis-tags: mechanisms of binding to Ni^{2+}-NTA surfaces'. In: *Journal of molecular recognition* 22.4 (2009), pp. 270–279. DOI: 10.1002/jmr.941.

[20] Lars Nieba et al. 'BIACORE Analysis of Histidine-Tagged Proteins Using a Chelating NTA Sensor Chip'. In: *Analytical Biochemistry* 252.2 (1997), pp. 217–228. DOI: 10.1006/abio.1997.2326.

[21] Suman Lata et al. 'High-Affinity Adaptors for Switchable Recognition of Histidine-Tagged Proteins'. In: *Journal of the American Chemical Society* 127.29 (2005), pp. 10205–10215. DOI: 10.1021/ja050690c.

[22] Virginia Platt et al. 'Influence of Multivalent Nitrilotriacetic Acid Lipid-Ligand Affinity on the Circulation Half-Life in Mice of a Liposome-Attached His_6-Protein'. In: *Bioconjugate chemistry* 21.5 (2010), pp. 892–902. DOI: 10.1021/bc900448f.

[23] Paul S. Cremer and Steven G. Boxer. 'Formation and Spreading of Lipid Bilayers on Planar Glass Supports'. In: *The Journal of Physical Chemistry B* 103.13 (1999), pp. 2554–2559. DOI: 10.1021/jp983996x.

[24] Edward T. Castellana and Paul S. Cremer. 'Solid supported lipid bilayers: From biophysical studies to sensor design'. In: *Surface Science Reports* 61.11 (2006), pp. 429–444. DOI: 10.1016/j.surfrep.2006.06.001.

[25] Sukit Leekumjorn and Amadeu K. Sum. 'Molecular Characterization of Gel and Liquid-Crystalline Structures of Fully Hydrated POPC and POPE Bilayers'. In: *Journal of Physical Chemistry* 111.21 (2007), pp. 6026–6033. DOI: 10.1021/jp0686339.

[26] Harald M. Seeger et al. 'Effect of Physical Parameters on the Main Phase Transition of Supported Lipid Bilayers'. In: *Biophysical Journal* 97 (2009), pp. 1067–1076. DOI: 10.1016/j.bpj.2009.03.068.

[27] Ruthven N.A.H. Lewis and Ronald N. McElhaney. 'Membrane lipid phase transitions and phase organization studied by Fourier transform infrared spectroscopy'. In: *Biochimica et Biophysica Acta (BBA) - Biomembranes* 1828.10 (2013), pp. 2347–2358. DOI: 10.1016/j.bbamem.2012.10.018.

[28] B.J. Litman, E.N. Lewis and I.W. Levin. 'Packing characteristics of highly unsaturated bilayer lipids: Raman spectroscopic studies of multilamellar phosphatidylcholine dispersions'. In: *Biochemistry* 30.2 (1991), pp. 313–319. DOI: 10.1021/bi00216a001.

[29] Fuyuki Tokumasu et al. 'Nanoscopic Lipid Domain Dynamics Revealed by Atomic Force Microscopy'. In: *Biophysical Journal* 84.4 (2003), pp. 2609–2618. DOI: 10.1016/s0006-3495(03)75066-8.

[30] Michel Grandbois, Hauke Clausen-Schaumann and Hermann Gaub. 'Atomic Force Microscope Imaging of Phospholipid Bilayer Degradation by Phospholipase A_2'. In: *Biophysical Journal* 74.5 (1998), pp. 2398–2404. DOI: 10.1016/S0006-3495(98)77948-2.

[31] Mario Brameshuber et al. 'Monomeric TCRs drive T cell antigen recognition'. In: *Nature Immunology* 19.5 (2018), pp. 487–496. DOI: 10.1038/s41590-018-0092-4.

[32] Federico Mazur et al. 'Liposomes and Lipid Bilayers in Biosensors'. In: *Nature Immunology* 19.5 (2018), pp. 487–496. DOI: 10.1038/s41590-018-0092-4.

[33] Holger Schönherr et al. 'Vesicle Adsorption and Lipid Bilayer Formation on Glass Studied by Atomic Force Microscopy'. In: *Langmuir* 20.26 (2004), pp. 11600–11606. DOI: 10.1021/la049302v.

[34] Joachim Rädler, Helmut Strey and Erich Sackmann. 'Phenomenology and Kinetics of Lipid Bilayer Spreading on Hydrophilic Surfaces'. In: *Langmuir* 11.11 (1995), pp. 4539–4548. DOI: 10.1021/LA00011A058.

[35] Chiho Hamai et al. 'Effect of Average Phospholipid Curvature on Supported Bilayer Formation on Glass by Vesicle Fusion'. In: *Biophysical Journal* 90.4 (2006), pp. 1241–1248. DOI: 10.1529/biophysj.105.069435.

[36] Reinhard Lipowsky and Udo Seifert. 'Adhesion of Vesicles and Membranes'. In: *Molecular Crystals and Liquid Crystals* 202.1 (1991), pp. 17–25. DOI: 10.1080/00268949108035656.

[37] Kay Terpe. 'Overview of tag protein fusions: from molecular and biochemical fundamentals to commercial systems'. In: *Applied microbiology and biotechnology* 60.5 (2003), pp. 523–533. DOI: 10.1007/s00253-002-1158-6.

[38] Wen-Hui K. Kuo and Howard A. Chase. 'Exploiting the interactions between poly-histidine fusion tags and immobilized metal ions'. In: *Biotechnology Letters* 33 (2011), pp. 1075–1084. DOI: 10.1007/s10529-011-0554-3.

[39] Mike Carson et al. 'His-tag impact on structure'. In: *Acta crystallographica. Section D, Biological crystallography* 63.Pt 3 (2007), pp. 295–301. DOI: 10.1107/S0907444906052024.

[40] Alan Chant et al. 'Attachment of a histidine tag to the minimal zinc finger protein of the Aspergillus nidulans gene regulatory protein Area causes a conformational change at the DNA-binding site'. In: *Protein Expression and Purification* 39.2 (2005), pp. 152–159. DOI: 10.1016/j.pep.2004.10.017.

[41] Sameh Magdeldin and Annette C. Moser. 'Affinity Chromatography: Principles and Applications'. In: 2012. ISBN: 978-953-51-0325-7. DOI: 10.5772/39087.

[42] William R. Kirk. 'Thermodynamics of imidazole-ligand binding to Ni-nitrilotriacetate in solution and covalently attached to agarose beads: Imidazole, his-6 (his-tag) peptide and a new bis-imidazolo-dithiane'. In: *Protein Expression and Purification* 95 (2014), pp. 1–7. DOI: 10.1016/j.pep.2013.11.008.

[43] Qi Xiao et al. 'Co-assembly of liposomes, Dendrimersomes, and Polymersomes with amphiphilic Janus dendrimers conjugated to Mono- and Tris-Nitrilotriacetic Acid (NTA, TrisNTA) enhances protein recruitment'. In: *Giant* 9 (2022), p. 100089. DOI: 10.1016/j.giant.2021.100089.

[44] Lawrence J. Stern and Don C. Wiley. 'Antigenic peptide binding by class I and class II histocompatibility proteins'. In: *Structure* 2.4 (1994), pp. 245–251. DOI: 10.1016/s0969-2126(00)00026-5.

[45] Pamela J. Bjorkman. 'MHC Restriction in Three Dimensions: A View of T Cell Receptor/Ligand Interactions'. In: *Cell* 89.2 (1997), pp. 167–170. DOI: https://doi.org/10.1016/S0092-8674(00)80195-6.

[46] Jerry. H. Brown et al. 'Three-dimensional structure of the human class II histocompatibility antigen HLA-DR1'. In: *Nature* 364.6432 (1993), pp. 33–39. DOI: 10.1038/364033a0.

[47] Christopher M. Dundas, Daniel Demonte and Sheldon Park. 'Streptavidin-biotin technology: improvements and innovations in chemical and biological applications'. In: *Applied microbiology and biotechnology* 97.21 (2013), pp. 9343–9353. DOI: 10.1007/s00253-013-5232-z.

[48] Johannes B. Huppa et al. 'TCR–peptide–MHC interactions in situ show accelerated kinetics and increased affinity'. In: *Nature communications* 463.7283 (2010), pp. 963–967. DOI: 10.1038/nature08746.

[49] René Platzer et al. 'Unscrambling fluorophore blinking for comprehensive cluster detection via photoactivated localization microscopy'. In: *Nature communications* 11.4993 (2020). DOI: 10.1038/s41467-020-18726-9.

[50] Avanti Polar Lipids. *16:0-18:1 PC (POPC)*. [Online] Available: https://avantilipids.com/product/850457 [Accessed: 29 September 2021].

[51] Avanti Polar Lipids. *18:1 DGS-NTA(Ni)*. [Online] Available: https://avantilipids.com/product/790404 [Accessed: 29 September 2021].

[52] Avanti Polar Lipids. *18:1 (Δ9-Cis) PE (DOPE)*. [Online] Available: https://avantilipids.com/product/850725 [Accessed: 29 September 2021].

[53] Lukas Schrangl. *sdt-python: Python library for fluorescence microscopy data analysis*. Version 15.2. https://doi.org/10.5281/zenodo.4604495. Oct. 2020. DOI: 10.5281/zenodo.4604495.

[54] Hazen Babcock, Yaron M. Sigal and Xiaowei Zhuang. 'A high-density 3D localization algorithm for stochastic optical reconstruction microscopy'. In: *Optical Nanoscopy* 1.6 (2012). DOI: 10.1186/2192-2853-1-6.

[55] Daniel B. Allan et al. *soft-matter/trackpy: Trackpy v0.5.0*. Version 15.2. https://doi.org/10.5281/zenodo.4682814. Apr. 2021. DOI: 10.5281/zenodo.4682814.

[56] Quanbo Jiang et al. 'Temperature Measurement in Plasmonic Nanoapertures Used for Optical Trapping'. In: *ACS Photonics* 6.7 (2019), pp. 1763–1773. DOI: 10.1021/acsphotonics.9b00519.

List of Abbreviations

AF647 Alexa Fluor 647

APC antigen-presenting cell

CCD charge-coupled device

CD cluster of differentiation

DGS-NTA(Ni) 1,2-dioleoyl-sn-glycero-3-[(N-(5-amino-1-carboxypentyl)iminodiacetic acid)succinyl] (nickel salt)

diSAV divalent Streptavidin

DOPE 1,2-dioleoyl-sn-glycero-3-phosphoethanolamine

EDTA ethylenediaminetetraacetic acid

GFP green fluorescent protein

His histidine

Hsp90 heat shock protein 90

JD Janus Dendrimer

LTC Lab-Tek chamber

MHC major histocompatibility complex

mSAV monovalent Streptavidin

NaOH sodium hydroxide

$NiCl_2$ Nickel(II)-chlorid

NTA nitrilotriacetic acid

pMHC peptide-major histocompatibility complex

POPC 1-palmitoyl-2-oleoyl-glycero-3-phosphocholine

sd standard deviation

SLB supported lipid bilayer

SMB single molecule brightness

SPR surface plasmon resonance

TCR T cell receptor

trisNTA trivalent nitrilotriacetic acid

triSAV trivalent Streptavidin

List of Figures

List of Tables

A. Values of the exponential fit of the background corrected intensity of the tracer lipid DOPE-Atto488

Table A.1.: Values of the exponential fits ($I = I_0 \cdot e^{-k_{off} \cdot t}$) to the background corrected intensity of the tracer lipid DOPE-Atto488. Temperature reflects the incubation temperature of the bilayer; Figure (row, column) describes the figure including row and column indices where the according exponential function is displayed; I_0 [counts/px] is the initial brightness value of the fit and k_{off} [min^{-1}] is the fitted off-rate; both values are displayed including the sd of the fit.

Temperature	Figure (row, column)	I_0 [counts/px]	k_{off} [min^{-1}]
21°C	4.3a) (1, 1)	13581.50 ± 92	$6.46 \cdot 10^{-24} \pm 4.2 \cdot 10^{-5}$
21°C	4.3a) (1, 2)	13533.25 ± 77.8	$(1.2 \pm 3.5) \cdot 10^{-5}$
21°C	4.3a) (1, 3)	13666.83 ± 95.6	$(7.3 \pm 4.2) \cdot 10^{-5}$
37°C	4.3b) (1, 1)	11894.24 ± 93.2	$(1.4 \pm 0.06) \cdot 10^{-3}$
37°C	4.3b) (1, 2)	11796.22 ± 101.7	$(1.1 \pm 0.07) \cdot 10^{-3}$
37°C	4.3b) (1, 3)	11108.48 ± 100.2	$(0.7 \pm 0.06) \cdot 10^{-3}$
37°C	4.3b) (2, 1)	8074.55 ± 92.7	$(0.8 \pm 0.09) \cdot 10^{-3}$
37°C	4.3b) (2, 2)	8330.46 ± 77.3	$(1.0 \pm 0.07) \cdot 10^{-3}$
37°C	4.3b) (2, 3)	8273.47 ± 77.1	$(0.7 \pm 0.06) \cdot 10^{-3}$
37°C	4.3b) (3, 1)	9118.63 ± 61	$(1.2 \pm 0.07) \cdot 10^{-3}$
37°C	4.3b) (3, 2)	9226.69 ± 100.7	$(1.5 \pm 0.1) \cdot 10^{-3}$
37°C	4.3b) (3, 3)	9143.62 ± 63.1	$(1.1 \pm 0.06) \cdot 10^{-3}$

B. Single molecule brightness values

Table B.1.: Resulting SMB values after filtering of localised data. One row corresponds to one experiment with the protein displayed in the first column. For IE^K two experiments were performed at 21°C: * was used to calculate surface density values in Figure 4.8a) (top, left), ** was used for the calculation of surface densities displayed in all other plots in Figure 4.8a). Temperature reflects the incubation temperature of the bilayer; Frame shows the number of frames from which molecules where considered for the brightness calculation; Mass reflects the filter setting of the intensity distribution; Background shows the filter setting of the background intensity distribution; Size [px] displays the filter setting of the size of the fitted Gaussian. SMB (mean ± sd) [counts/signal] shows the mean brightness after filtering.

Protein	Temperature	Frame	Mass	Background	Size [px]	SMB (mean ± sd) [counts/signal]
IE^K	21°C	$10-99$	≤ 10000	≤ 260	$0.75-1.25$	$3985.09 \pm 2140.30^*$
IE^K	21°C	$10-99$	≤ 4200	≤ 240	$0.75-1.25$	$1713.57 \pm 1044.37^{**}$
IE^K	37°C	$10-99$	≤ 3800	≤ 225	$0.75-1.25$	1106.45 ± 379.77
triSAV	21°C	0	≤ 27000	≤ 270	$0.75-1.25$	10901.22 ± 493.74
triSAV	37°C	0	≤ 7000	≤ 250	$0.75-1.25$	3072.94 ± 1446.32
diSAV	21°C	0	≤ 12500	≤ 250	$0.75-1.25$	5117.63 ± 2612.72
diSAV	37°C	0	≤ 3500	≤ 240	$0.75-1.25$	1816.69 ± 721.01
mSAV	21°C	$10-99$	≤ 10000	≤ 235	$0.75-1.25$	3604.61 ± 1942.95
mSAV	37°C	$10-99$	≤ 3000	≤ 235	$0.75-1.25$	1458.93 ± 511.00
IE^K (NTA recharging)	37°C	$10-99$	≤ 3500	≤ 255	$0.75-1.25$	1247.23 ± 417.39
IE^K (pH dependence)	37°C	$10-99$	≤ 2700	≤ 250	$0.75-1.25$	1303.05 ± 449.89

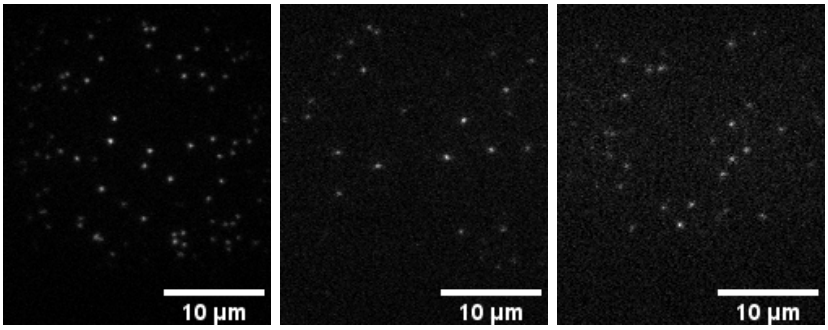

(a) (b) (c)

Figure B.1.: Exemplary image of a bilayer functionalised with IE^K at a) 21°C*, b) 21°C**, c) 37°C. * was used to calculate surface density values in Figure 4.8a) (top, left), ** was used for the calculation of surface densities displayed in all other plots in Figure 4.8a). The 10^{th} image frame is shown, since localisations are considered from this frame on for the SMB calculation. Images have different brightness scales.

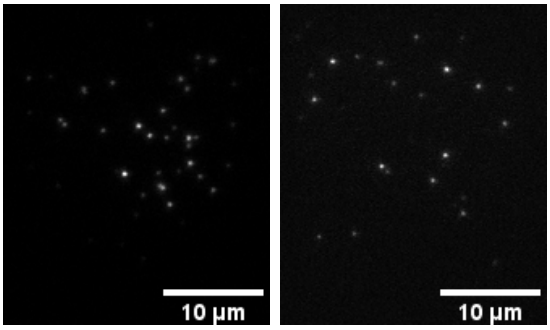

(a) (b)

Figure B.2.: Exemplary image of a bilayer functionalised with triSAV at a) 21°C and b) 37°C. The first image frame is shown, since only localisations from this frame are considered for the SMB calculation. Images have different brightness scales.

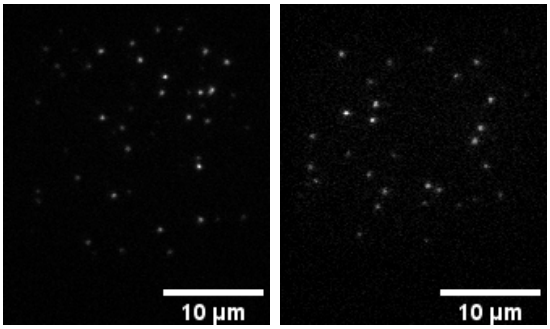

(a) (b)

Figure B.3.: Exemplary image of a bilayer functionalised with diSAV at a) 21°C and b) 37°C. The first image frame is shown, since only localisations from this frame are considered for the SMB calculation. Images have different brightness scales.

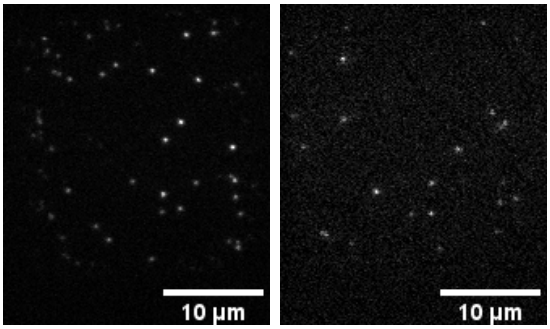

(a) (b)

Figure B.4.: Exemplary image of a bilayer functionalised with mSAV at a) 21°C and b) 37°C. The 10^{th} image frame is shown, since localisations are considered from this frame on for the SMB calculation. Images have different brightness scales.

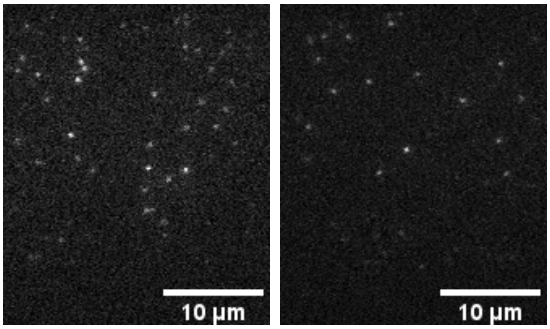

(a) (b)

Figure B.5.: Exemplary image of a bilayer functionalised with IE^K at 37°C a) in the experiment where NTA binding sites of high density bilayers were recharged and b) in the experiment were the HBSS buffer pH was altered. The 10^{th} image frame is shown, since localisations are considered from this frame on for the SMB calculation. Images have different brightness scales.

C. Values of the exponential model fitted to protein surface densities

Table C.1.: Values of the exponential model (Equation 4.3) fitted to protein surface densities of a) IE^K, b) triSAV, c) diSAV, d) mSAV, e) IE^K after NTA recharging with $NiCl_2$, f) IE^K with different buffer pH. Temperature reflects the incubation temperature of the bilayer; Figure describes the figure where the according density values and exponential function are displayed; RL_0 [signals/µm^2], k_{off} [min^{-1}] and RL_{const} [signals/µm^2] reflect the determined fit value including standard deviation.

(a) IE^K

Temperature	Figure	RL_0 [signals/µm^2]	k_{off} [min^{-1}]	RL_{const} [signals/µm^2]
21°C	4.8a) (top, left)	102.8 ± 1.5	$(4.7 \pm 0.2) \cdot 10^{-3}$	-
21°C	4.8a) (top, right)	39.5 ± 1.4	$(2.3 \pm 0.2) \cdot 10^{-3}$	-
21°C	4.8a) (bottom, left)	169.9 ± 3.7	$(3.4 \pm 0.2) \cdot 10^{-3}$	-
21°C	4.8a) (bottom, right)	13.7 ± 0.6	$(4.5 \pm 0.3) \cdot 10^{-3}$	-
37°C	4.8b) (left)	201.5 ± 3.9	$(3.3 \pm 0.1) \cdot 10^{-2}$	1.7 ± 1.1
37°C	4.8b) (middle)	186.6 ± 4.6	$(2.6 \pm 0.2) \cdot 10^{-2}$	6.1 ± 1.7
37°C	4.8b) (right)	244.5 ± 1.1	$(5.4 \pm 0.2) \cdot 10^{-2}$	1.2 ± 0.3

(b) triSAV

Temperature	Figure	RL_0 [signals/µm²]	k_{off} [min^{-1}]	RL_{const} [signals/µm²]
21°C	4.12a) (left)	22.5 ± 0.4	$(1.1 \pm 0.1) \cdot 10^{-2}$	14.2 ± 0.4
21°C	4.12a) (middle)	16.4 ± 0.6	$(1.8 \pm 0.1) \cdot 10^{-2}$	10.2 ± 0.3
21°C	4.12a) (right)	24.8 ± 0.5	$(1.0 \pm 0.1) \cdot 10^{-2}$	14.7 ± 0.5
37°C	4.12b) (left)	85.6 ± 3.8	$(2.3 \pm 0.2) \cdot 10^{-2}$	13.1 ± 1.5
37°C	4.12b) (middle)	48.3 ± 1.7	$(2.0 \pm 0.1) \cdot 10^{-2}$	8.7 ± 0.6
37°C	4.12b) (right)	39.3 ± 0.7	$(1.4 \pm 0.1) \cdot 10^{-2}$	4.1 ± 0.4

(c) diSAV

Temperature	Figure	RL_0 [signals/µm²]	k_{off} [min^{-1}]	RL_{const} [signals/µm²]
21°C	4.16a) (left)	51 ± 0.7	$(1.9 \pm 0.1) \cdot 10^{-3}$	-
21°C	4.16a) (middle)	44.6 ± 0.6	$(1.1 \pm 0.1) \cdot 10^{-3}$	-
21°C	4.16a) (right)	37.6 ± 0.7	$(0.7 \pm 0.1) \cdot 10^{-3}$	-
37°C	4.16b) (left)	114.8 ± 3.5	$(2.6 \pm 0.2) \cdot 10^{-2}$	5.3 ± 1.9
37°C	4.16b) (middle)	233.6 ± 17.7	$(5.1 \pm 0.3) \cdot 10^{-2}$	4.6 ± 0.8
37°C	4.16b) (right)	164.6 ± 9.5	$(2.4 \pm 0.2) \cdot 10^{-2}$	6.5 ± 2

(d) mSAV

Temperature	Figure	RL_0 [signals/µm²]	k_{off} [min^{-1}]	RL_{const} [signals/µm²]
21°C	4.20a) (left)	268.4 ± 5.7	$(5.3 \pm 1.4) \cdot 10^{-4}$	-
21°C	4.20a) (right)	233.1 ± 2.3	$(5.9 \pm 0.7) \cdot 10^{-4}$	-
37°C	4.20b) (left)	281.1 ± 14.9	$(1.2 \pm 0.2) \cdot 10^{-2}$	$5.6 \cdot 10^{-15} \pm 15.3$
37°C	4.20b) (middle)	244.4 ± 11.4	$(1.6 \pm 0.2) \cdot 10^{-2}$	$1.7 \cdot 10^{-15} \pm 5.1$
37°C	4.20b) (right)	297.4 ± 12.5	$(1.3 \pm 0.1) \cdot 10^{-2}$	$3.2 \cdot 10^{-13} \pm 7.5$

(e) IE^K with NTA recharging

Temperature	Figure	RL_0 [signals/μm^2]	k_{off} [min^{-1}]	RL_{const} [signals/μm^2]
37°C	4.24 (left)	63.1 ± 3	$(7.0 \pm 0.3) \cdot 10^{-2}$	2.3 ± 0.1
37°C	4.24 (middle)	78.9 ± 3.2	$(5.8 \pm 0.2) \cdot 10^{-2}$	2.6 ± 0.1
37°C	4.24 (right)	78 ± 4.5	$(3.4 \pm 0.2) \cdot 10^{-2}$	2.3 ± 0.3

(f) IE^K in dependence on buffer pH

Temperature	Figure	RL_0 [signals/μm^2]	k_{off} [min^{-1}]	RL_{const} [signals/μm^2]
37°C	4.28 (left)	111.6 ± 4.6	$(2.3 \pm 0.2) \cdot 10^{-2}$	1.8 ± 1.9
37°C	4.28 (middle)	203.3 ± 9.7	$(6.5 \pm 0.2) \cdot 10^{-2}$	4.9 ± 1.7
37°C	4.28 (right)	40.2 ± 1.8	$(1.5 \pm 0.2) \cdot 10^{-2}$	13 ± 0.9
37°C	4.28 (right)	43.3 ± 1.3	$(5.8 \pm 0.3) \cdot 10^{-3}$	-